REPUBLIC OF TURKEY

ALTINBAS UNIVERSITY

Institute of Graduate Studies

Mechanical Engineering

ANALYSIS OF BIONIC STRUCTURAL DESIGN OF FRONT CAR BUMPER USING FINITE ELEMENT METHOD

Haider AbdulAmeer Abbas AL-ATTRI

Master’s Thesis

Supervisor

Asst. Prof. Yaser ALAIWI

Istanbul, 2022

ANALYSIS OF BIONIC STRUCTURAL DESIGN OF FRONT CAR BUMPER USING FINITE ELEMENT METHOD

Haider AbdulAmeer Abbas AL-ATTRI

Mechanical Engineering

Master’s Thesis

ALTINBAŞ UNIVERSITY

2022

The thesis titled "ANALYSIS OF BIONIC STRUCTURAL DESIGN OF FRONT CAR BUMPER USING FINITE ELEMENT METHOD" prepared by "HAIDER ABDULAMEER ABBAS AL-ATTRI" and submitted on 13/12/2022 has been **accepted unanimously** for the degree of Master of Science in Mechanical Engineering.

____
Asst. Prof. Dr. Yaser ALAIWI

the Supervisor

Thesis Defense Committee Members:

Asst. Prof. Dr. Yaser ALAIWI	Department of Mechanical Engineering, Altınbaş University	___________________
Asst. Prof. Dr. Serdar AY	Department of Mechanical Engineering, Altınbaş University	___________________
Asst. Prof. Dr. Haydar İzzettin KEPEKÇİ	Department of Mechatronic Engineering, Nişantaşı University	___________________

I hereby declare that this thesis meets all format and submission requirements of a Master's Thesis.

Submission date of the thesis to Institute of Graduate Studies: ___/___/___

I hereby declare that all information/data presented in this graduation project has been obtained in full accordance with academic rules and ethical conduct. I also declare all unoriginal materials and conclusions have been cited in the text and all references mentioned in the Reference List have been cited in the text, and vice versa as required by the abovementioned rules and conduct.

Haider AbdulAmeer Abbas AL-ATTRI

Signature

DEDICATION

I dedicate this project to everyone who had the credit to complete it, foremost among them is the research supervisor, Dr. Yaser ALAIWI, who stood with me step by step and my parents ask Allah to keep them.

ACKNOWLEDGEMENTS

For all of his help, support, and understanding when I was a student under the tutelage of Asst. Prof. Dr. Yaser ALAIWI, I am grateful. Having a supervisor who really cared about my job and reacted quickly to my questions and concerns was a wonderful blessing. In addition, I'd want to express my gratitude to the Altinbaş University employees that helped me complete this project.

ABSTRACT

ANALYSIS OF BIONIC STRUCTURAL DESIGN OF FRONT CAR BUMPER USING FINITE ELEMENT METHOD

Al-Attri, Haider

M.Sc., Mechanical Engineering, Altınbaş University,

Supervisor: Asst. Prof. Yaser ALAIWI

Date: 12/2022

Pages: 103

In this study, the energy absorption impact of bionic bumpers has been analyzed using nonlinear finite element simulation. In a frontal collision, a moving rigid wall was used to impact the bumper beam. The design of the bionic structure was based on the 2019 KIA (optima) model, with the cross-sectional shape modified to a honeycomb structure. Computer simulations demonstrate that the design of bionic bumpers increases the absorbed energy of a bumper during high-velocity collisions. Changes in stresses and strains were also observed throughout the impact.

The construction included the structural components of the 2019 KIA optima bumper's Honeycomb bumper and was made of a different kind of material (stainless steel AISI 304 and AL 7003). The results indicate that the bionic design improves the bumper's specific energy absorption (SEA). The stress and strain contours, the displacement of the node, which is on the deformation parts of the bumper beam, the amount of compression of the crash box, the process of energy conversion, etc. The maximum crush deformation of the Honeycomb (ST AISI304) cross-beam and box bumper models was reduced by a decrease of 47.18% and for (AL 7003) the reduction was less than (AISI304) by 11.089 %. As for the energy absorption capacity under the lateral impact, a bionic design can be used in the future bumper body.

Finally, the thesis discusses the influence of factors on collision characteristics, such as the section shape and material properties of the bumper beam. The design and analysis of the bumper beam were subjected to offset impact loading using ANSYS-Explicit dynamics and suggested the best shape design. Also, the three bumpers' natural frequencies and mode shapes have been calculated.

Keywords: Impact, Honeycomb, Bumper, Explicit Dynamics, High Velocity.

TABLE OF CONTENTS

Pages

LIST OF TABLES

Pages

LIST OF FIGURES

Pages

ABBREVIATIONS

FE	:	Finite Element
CAD	:	Computer-Aided Design
CAI	:	Computer-Aided Instruction
E.C.E.	:	United Nations Agreement
GMT	:	Glass Mat Thermoplastic
SMC	:	Sheet Molding Compound
FGF		Functionally Graded Foam
UF		Urea-Formaldehyde Foam
FFT		Fast Fourier Transform
FMVSS		Federal Motor Vehicle Safety Standards
DOE		Design Of Experiments
RSM		Response Surface Models
DHP		Double Hat Profile
BBT		Bionic Crush Force

LIST OF SYMBOLS

U	:	Strain energy
U_0	:	Strain energy density
ε	:	Equivalent strain
ε^e	:	Elastic strain
ε^p	:	Plastic strain
v	:	Poisson ratio
N	:	Strain hardening exponent
U_d	:	Distortion energy density
σ_y	:	Yield stress
σ_{yt}	:	Tensile yield stress
σ_{yc}	:	Compression yield stress
σ_{VM}	:	Von mises stress
σ_z	:	Aaxial stress
$\sigma_{1,2,3}$	:	Pprinciple stress
E	:	Young's modulus
E_t	:	Tangent modulus
F	:	Force
d	:	Distance
v	:	Velocity

ΔE : Stands for the loss of mechanical energy after a collision

u : Displacement

$\ddot{u}$: Acceleration

ω : Natural frequency

M : Spring mass system

K : Stiffness of spring

1. INTRODUCTION AND PURPOSE

Car accidents are on the rise due to manufacture on a mass scale of autos and utilities, and the status of the car accidents in a range of collision probabilities is the worst. Bumper beams are utilized as shock absorbers in the automobile industry. They were joined to the front and rear ends of automobiles using brackets that act as absorber boxes by carrying a majority of the axial stresses. By absorbing crash energy, these parts are meant to keep the car from getting damaged and to keep passengers from getting hurt [1].

The front of the car is where the bumper beam gets attached. It’s a vital component that helps keep that the structure over time and distributes stress throughout. So, the current bumper beam systems are an important part of a car's safety concept because they make sure that passengers only feel small accelerations. Also, there is a need for long-lasting shock absorber systems that work well and crash in the same way every time [2].

A car's bumper is typically made up of four main components: the fascia, reinforcement beam, absorber box, and mounting system [3]. Under the bumper, the cross-section beam receives lateral pressure loads and is often a thin-walled construction. The thin-walled section has been the subject of several research as a means of bringing the horizontal compressive stress into a more manageable [4]. The term "crashworthiness" is used to describe how well they operate in adverse conditions, such as being subjected to high impact forces, when the impact of a collision is mitigated thanks to the bumper beam's improved performance. Their impact performance might be improved by altering their cross-sectional profile. To do this, it is necessary to construct a detailed simulation of the bumper's behavior in a collision before making any adjustments to the physical design [5].

With the rise in worldwide car ownership, the frequency of traffic accidents is also on the rise, causing irreversible harm to individuals and their property [6]. Statistics show that frontal collisions account for the vast majority of all car accidents [7]. The front bumper system is the first part of the vehicle to make contact with an object in a head-on collision. Consequently, studying the bumper system is crucial to better the vehicle's crashworthiness and avoid injuries to pedestrians. Most modern studies of bumper systems aim to improve crashworthiness by improving the structure or utilizing special materials. The basic method to reinforce the structure is to enhance the form or thickness of the components of the bumper system [8].

An automobile's bumper, B pillar, and side-door beam can all serve to deflect or absorb the force of an accident, protecting the lives of those inside. The bumper receives lateral impact loading during the collision process. A bumper's primary function is to absorb some of the energy from a crash to keep the vehicle's occupants alive [3]. A car’s bumper is composed of four components: the crushable column, the fascia, the crash box, and the cross- beam. It is common practice to provide a lateral compression load to the cross- beam located under the bumper. There has been a lot of research on thin-walled constructions under horizontal compression straightening. Thin-walled structures are useful energy absorbers for experiments, analyses, and computational models [9].

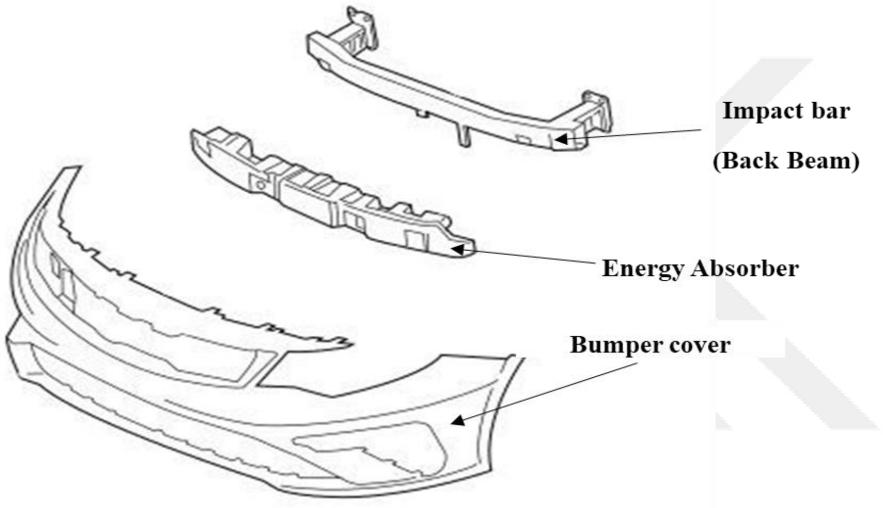

Figure 1.1: Schematic of 2019 Kia optima the bumper [10]

Front bumper systems in vehicles are fitted with sophisticated energy-absorbing systems to protect pedestrians and passengers in low-speed accidents [11].

However, pedestrian safety systems and bumper systems have vastly distinct force and impact energy requirements. The energy absorber in a foam bumper, for instance, may be too rigid to prevent serious injury in the event of a collision with a pedestrian's lower limbs due to the tremendous force involved. But it's very similar in character. Furthermore, conventional energy absorbers are typically integrated structures made of thermoplastic polymer or foamed polypropylene (EPP), both of which may require repairs owing to localized damage [12].

This study aimed to improve physical comprehension of the many phenomena that happen during the compensating effect of a longitudinal system of a vehicle bumper beam and to evaluate the modeling process for the collision performance of the system. In the presented work, an attempt was made the process of building a Finite Element Model of bumper beam with the appropriate bend using a modulation simulation.

1.1 BUMPER PARTS AND MATERIALS

A bumper is a protective bar mounted on the front and back of a car or truck that absorbs impact and shields its occupants. In the case of an accident, the bumper absorbs the force of the collision and protects the vehicle's front and back [13].

The bumper is a long, horizontal bar that can either be integrated into the design of the exterior of the vehicle or it can protrude from the front or the rear of the vehicle. All new cars, trucks and SUVs are manufactured with front and rear bumpers – as these are necessary safety parts to protect passengers from collisions [8].

A bumper consists of four components:

a. Bumper cover: Different kinds of plastics are used to make bumpers for cars. Polyamides, polypropylene, Polycarbonates, polyesters, thermoplastic olefins, and polyurethanes, or TPOs, are some of the most common. Many bumpers are made of a mix of these different materials.

Figure 1.2: Bumper cover [8].

b. The bumper absorber: Behind the plastic bumper cover that looks nice is where the bumper absorber is. As its name suggests, the bumper absorber takes up the energy of a collision so that the body and mechanical parts behind it aren't damaged. It is made to be a "sacrificial" part, which means that if it gets damaged in a crash, it must be replaced. Most of the bumper systems on passenger cars in North America today are made up of a steel, aluminum, or composite reinforcement bar and an energy-absorbing material. Expanded polypropylene foam is the most important type of material for energy-absorbing structures (EPP).

Figure 1.3: The bumper absorber [8].

c. The bumper reinforcement bar: This part is usually called the "impact bar," "reinforcement bar," or "bumper reinforce," and it works with the "absorber pad," which is often made of Styrofoam or plastic and is missing or hard to see in your picture. Together, they make a modern bumper safe. The bumper reinforcement is made of a high-performance material, like steel, aluminum, or plastic, and is made to protect your car or truck from the front or back.

Figure 1.4: The bumper reinforcement bar [8].

Impact bars assist in increasing the safety of automobiles in case of a collision. Impact bars are specialized mechanical devices that disperse the force of an impact across a large surface area. Because the bar is shaped like a rectangle, any weight that hits it is spread out evenly over its whole surface.

d. The bumper mounting system: A bumper bracket is the component responsible for securing the bumper to the vehicle. Usually more than one, these metal pieces fasten to the front and side rails of your vehicle's chassis. In the aftermath of a collision, you should replace the brackets that hold your bumper in place.

Figure 1.5: The bumper mounting system [8].

1.2 BIONIC STRUCTURE

The contemporary design process is increasingly characterized by approach of a holistic. This approach to design incorporates several tenets of sustainable development, is an interdisciplinary design approach that seeks synergistic solutions. In this way, bionic design, which allows, the functional properties of biological tissues, the mapping of nature's rules, as well as processes and structures, is important for transferring the developed models to technology. Bionic architecture is made up of things that are good for the environment because they are made to fit their surroundings and use the least amount of energy and materials possible [14].

The biological architecture of the natural world must change to fit the conditions it encounters. Water and nutrients can be transported from the roots to the leaves thanks to the plant's many components, many of which are light and have high mechanical qualities [15].

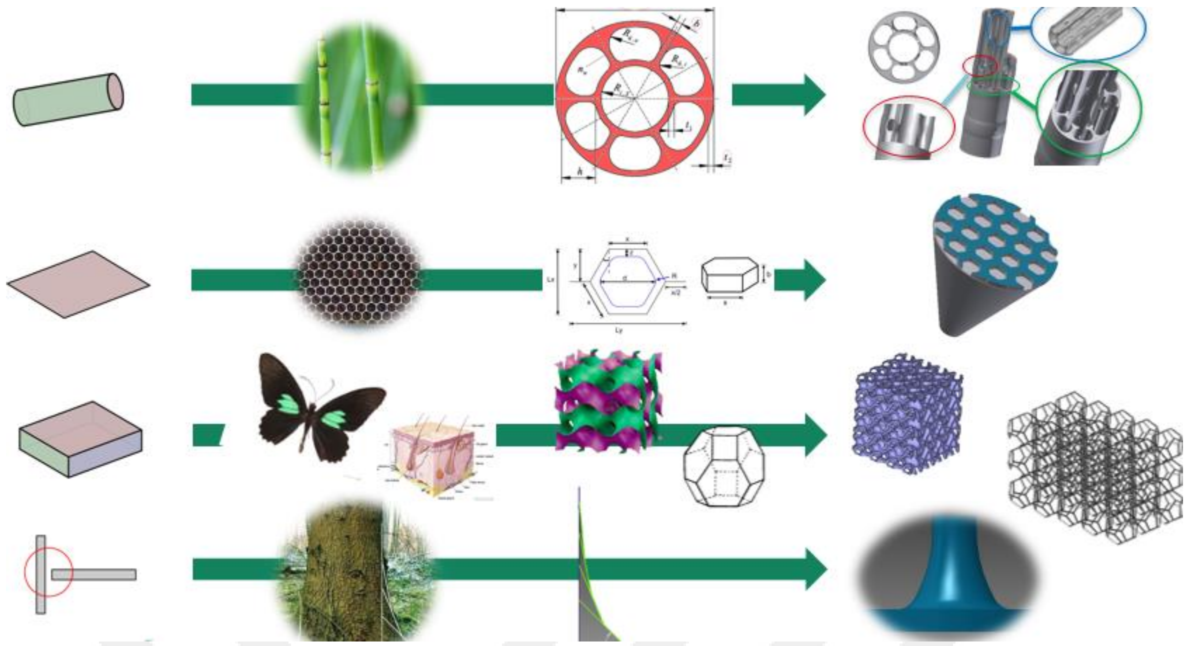

Figure 1.6: CENIT is creating an automated bionic-design toolset, using structure inspiration drawn from natural forms. [16].

1.3 VEHICLE BUMPER BEAM

Bumper beams are structural elements that can be found in either the front or the rear of a car. it helps to absorb collision energy and resist bending in both low-impact and high-impact collisions to reduce damage and keep people and other vehicles safe. they can be made of steel, aluminum alloys, plastic, or other materials. using composite materials to make bumper beams makes them lighter, which means they use less fuel, which is the most important challenge of this century [17]. The Kia K5, which used to be called the Kia Optima, is a mid-size car made by Kia since 2000 and sold all over the world under different names. Kia was chosen for this study because it is so common on the streets of Iraq and because it is not very durable [17]

Figure 1.7: The 2019 Kia Optima design.

Table 1.1: The KIA Optima 2019 Specifications list [17].

2019 Kia Optima Specifications			
Engine		**Exterior Dimensions**	
Type	2.4L I-4, (GDI)	**Wheelbase (in.)**	110.4 in.
Displacement (cc)	2,359 cc	**Length (in.)**	191.1 in.
Bore x stroke (mm)	88.0 x 97.0	**Width (in.)**	73.2 in.
Compression Ratio	11.3:1	**Height (in.)**	57.7 in.
Horsepower	185 HP @ 6,000	**Track, front/rear (in.) - 16-inch**	63.5 in. / 63.8 in.
Torque	178 lb-ft @ 4,000	**Track, front/rear (in.) - 17-inch**	63.1 in. / 63.4 in.
Head	Aluminum	**Min. Ground Clearance (in.)**	5.3 in.
Fuel Injection System	Gasoline Direct Injection (GDI)	**Curb Weight**	
Rec. Fuel	Unleaded Gasoline	**6-Speed Automatic Transmission**	3,230 lbs.
Fuel tank capacity (gal.)	18.5 gallons	**Weight Distribution (Front / Rear)**	61% / 39%

1.4 RESEARCH OBJECTIVE

This paper aims to investigate the car's front bumper existing in the Iraqi market and to propose design improvements to it using Impact Analysis to satisfy the following objectives.

a. Recreating the effects of a collision at the beam's center requires modeling and simulation of a beam from an existing automobile bumper.

b. Production of parameters for designing bumpers that are more resistant to shocks using bionic cross-section designs in simulation.

c. Propose ideas for a bumper beam that will absorb the impact energy of cars going at high speeds (120 km/hr.).

d. Comparing the present bumper design with several cross-section designs and adjusting for crashworthiness.

e. Conducting a full-size static force deformation test for the original car bumper, in order to see the shape and value of the deformation that occurred when the bumper was exposed to a direct collision.

2. LITERATURE REVIEW

2.1 INTRODUCTION

We talk about a summary of the relevant studies and papers. As you can see, they've been neatly stacked in chronological order. Where analysis of collisions, improved material characteristics, and new designs for the bumper beam were among the issues that were studied and analyzed by the researchers, as well as making simulations on some CAI programs such as ANSYS, ABAQUS, ALTAIR software etc.

2.2 LITERATURE REVIEW

Many studies have studied the bumper beam, its design, and the improvements that have been made in terms of increasing impact resistance or improving the rate of energy absorption resulting from the collision by making a change in the geometry or adding materials with a high rate of energy absorption. Among these researches:

In this work Americas designed a front bumper system for a car that prioritizes passenger safety while yet providing enough protection in the event of a collision at 5 miles per hour. Design problems included meeting the requirements for a large "soft" crush area and low barrier penetration. Using computer modeling, a solution for the front bumper of a sport utility vehicle was created that balances these design requirements. MADYMO was used to simulate a pedestrian upper leg form to bumper test, while LS-DYNA3D was used to simulate 5 mph barrier test simulations. The performance of the digitally designed pedestrian bumper device was proven by physical testing. This study will describe the procedure and strategies utilized to design this pedestrian bumper device. Some information on the new bumper's design and performance will be presented [18].

The study presents the construction of a school bus FE model that is then employed in a number of different kinds of calculations. The model's construction mirrored that of a school bus, and it was designed to replicate the behavior of such a vehicle in a variety of crash scenarios. It had sufficient detail to guarantee trustworthy results and was still usable with current gear. For the purpose of testing the school bus model and simulating collisions with full-scale FE vehicle models employed as bullet vehicles, the commercial explicit FE method LS-DYNA was utilized. In this article, we analyze the typical duration of a variety of situations. Typically, the back or side of a vehicle is affected in collisions that last just a few hundred milliseconds [19].

In this study, extensive research was done on pedestrian safety with the end goal of informing legislative action. Designing car hoods and bumpers to prevent pedestrians from being injured in collisions is important. The safe constructions of the hood and bumper are designed using two analytical methods: an actual experiment and a computer simulation. A genuine experiment would cost a lot of money, and computer simulations include errors in the way they model things. Amassing all of the experimental data to determine the design trend is a good idea. However, due of the constraints of most budgets, computer simulation is frequently employed. As part of this study, a technique is developed that makes use of both experimental and simulated data. When combining the two approaches, orthogonal arrays are used as a connecting mechanism. In an orthogonal array, only a subset of rows undergoes actual tests, while the remainder is instead replaced by computer simulations. Each test should involve a unique set of conditions. Errors in mathematics are examined. A hood and bumper are manufactured using current technologies to safeguard pedestrians. Both physical experiments and computational simulations are carried out for orthogonal array rows. The findings demonstrate a reasonable distribution of errors and a well-executed design [20].

According to the E.C.E. UNITED NATIONS AGREEMENT, this project seeks to apply an LS-DYNA ANSYS 5.7 impact model to examine and evaluate a commercial front bumper beam made of glass mat thermoplastic (GMT). The design was driven by factors like shape, substance, and impact conditions, with results compared to those of more common metals like steel and aluminum. The last distinguishing feature is the strong SMC that comes highly recommended. Crash testing on the model demonstrates that it is as strong and rigid as metals and composites, but requires less material, is simpler to manufacture because to its simplified geometry, and is less expensive to produce [21].

Here, we describe the findings of a computational investigation in which we investigated the effects of impact loads that were shifted by 40% along the longitudinal axis of bumper beams. Through the use of the non-linear finite element technique LS-DYNA, simulations were carried out in an effort to come up with a numerical description of the system's behavior that was superior, more effective, and more reliable. An industrial-style modeling approach and a user-defined material model process were compared, and we discussed the differences and similarities between the two. This second approach is premised on a model of the material that incorporates characteristics of the material such as ductile fracture criteria, isotropic strain, and strain-rate hardening. Shell and solid elements of the longitudinal design of the bumper beam were distinguished in a clear and distinct manner. The rate of energy dissipation was consistent with the experimental results, as was the overall deformation pattern that was predicted by the findings of the computer simulation of the accident. The models were able to effectively estimate the collapse mode seen in real testing, with one exception: the bumper beam-longitudinal system employing AA7003-T1 longitudinal. In the sensitivity studies, both physical and numerical factors were taken into consideration. Adaptive meshing was one of the numerical characteristics that was investigated, while the impacts of strain rate and the heat-affected zone were some of the physical parameters that were looked at [22].

Accident bending tests were performed on both foam-filled and unfilled square aluminum beams, and the results were evaluated using the finite element technique. The strength and resilience of the square aluminum beams were improved to withstand the greatest possible impact. In this way, the required quantity of energy was taken in. After much investigation into foam's potential for use in reinforcing filled beams, the optimum foam-filled beam was found using the optimization method; this beam is equally effective at energy absorption as optimal empty tubes but weighs much less [23].

The work's frontal structure consists of the bumper system and a crash box that connects the bumpers to the body of the automobile. FMVSS part 581 and the lower-leg form impact test for pedestrian safety have both been meticulously considered in the design of the bumper system. The two rules have different requirements for how stiff the bumper system must be. A soft bumper system is needed to protect the lower leg, while a stiffer system is usually required to withstand the impact of the pendulum. Here, we present an improved bumper system and use the nonlinear finite element approach to study its dynamics. An optimization problem is formulated using the study' findings. There are two loading criteria that are employed, and each rule is interpreted as a restriction based on that condition. One approach to dealing with this predicament is to optimize a response surface approximation. When an incident occurs, RCAR dictates that the associated repair costs must decrease. Crash boxes can absorb energy in the event of a low-velocity collision, which might drastically cut down on repair expenses. Non-linear finite elements are used to determine the crash box's robustness. The results of the research are utilized to define a crash box optimization issue. A discrete design based on an orthogonal array is used to solve this issue on a flat surface [24].

In this paper, analyze the concept that underlies the development of the fiber-reinforced epoxy composite bumper absorber. This research paper explains how bumpers made of a composite material might mitigate the effects of pedestrian collisions. The inspiration for the design comes from systematically applying proven concepts, with the best of these serving as the basis for the final product. The number of energy absorbers needed in a design can be determined via testing the absorber. The optimal construction details for a composite material, circular energy absorber with holes on both ends were analyzed. The energy absorber's attachment to the bumper and the fascia were also looked into. In this study, a fiber-reinforced epoxy composite was tested with a quasi-static compression method to determine its reversible energy absorption properties. In cases of low impact, such as those involving pedestrians, the composite absorber might have substituted more traditional materials like EPP foam. The fiber orientation at [452,03,901] looks to be optimal for this purpose, and the absorber's dimensions are 150 mm in length and 75 mm in width [25].

This study analyzes the material, thickness, form, and impact condition of a car's front bumper beam with the goal of improving its crashworthiness in the case of a low-velocity collision. In order to determine whether or not the original bumper complies with the E.C.E. United Nations Agreement, Regulation No. 42, 1994, we conduct crash tests on a dummy vehicle. The purpose of this investigation is to examine the relative strength of aluminum bumper beams and composite beams. You can measure how well the elasticity mode absorbs energy and resists impact force by how much it bends. Impact force, deflection, energy absorption, and stress distribution are modeled and evaluated for a composite front bumper beam made from aluminum, glass mat thermoplastic (GMT), and high-strength sheet molding (SMC). We've considered all of the possible variations in material, form, and wall thickness in our hunt for the best solution. The findings suggest a revised SMC bumper beam could improve upon previous designs in terms of impact energy, deflection, and stress distribution, all while using less elastic strain energy. It is also being looked into how passengers affect the dynamics of an accident. Estimated parameters are compared graphically over time. Advantages of SMC include its low unit cost and small weight (no ribs equal less work) (made of cheap components) [26].

This article investigated a hollow tube-like beam reinforced with ribs for car bumpers. We may compare the crashworthiness of the rib-reinforced beam to thin-walled hollow tube-like beams filled with and without foam by modelling their bending behavior under impact loads (empty beam and foam-filled beam). The reinforcement's revised profile reduces the bending force and increases the rib's energy absorption. energy absorption, specific energy absorption, and early peak force reduction are crashworthiness optimization objectives utilizing the optimum point approach (IPM). Normalized cubic spline functions find the best rib design. Rib-reinforced beams absorb more energy and create less crash force than empty and foam-filled beams of the same weight. Ribbed beams absorb strain better because their rumples are tighter around the beam's depressed depression [27].

The bumper of the vehicle, a crucial part, was the focus of this research and development. There is growing pressure on bumper manufacturers to reduce product weight while still meeting all applicable crashworthiness and safety regulations. The engineering process begins with the CAD design of an automobile's bumper subsystem and extends to the development of a generic assembly model, multi-attribute simulation models, meshes, and the specification of several analysis scenarios. Successful optimization relies heavily on the procedure's ability to automatically iterate through design and model improvements, and this is made feasible by the procedure's inherent associativity. The model is constructed based on the geometric and cross-sectional information of the structural bumper. The Design of Experiments (DOE) approach is an effective means of pinpointing the most critical design parameters. The weight of the vehicle's bumper is then minimized utilizing controllable RSMs to fulfill all design requirements [28].

As mandated by the European Economic Community and the Federal Motor Vehicle Safety Standards, this study optimizes a vehicle's bumper beam design to reduce pedestrian injuries in a collision at 5 mph in front of a hard wall. Intermediate response surface modeling was used to mimic bumper impact study non-linear force-displacement curves (IRSM). IRSM models' accuracy was compared to 3D nonlinear finite element model results. 3% separated the two categories in largest distance. Placket-Burman theory was used to estimate a pedestrian's lower leg's impact response value functions. The bumper component was improved using the indicated design technique to protect pedestrians from bumper-related lower leg injuries and account for 5 mph front rigid-wall accidents [29].

In this study, we investigate the use of numerical analysis to create a model of a low-velocity head-on collision. Parametric assessments of low-velocity collisions and estimates of the severity of low-velocity collisions that have already happened were both possible using this model. Bumper is portrayed as a flexible attachment to what is thought to be a rigid chassis. The model's theoretical foundations are in Newtonian physics. The amount of impact force required to achieve a desired deformation is calculated with the help of a special function in the model, dubbed the impact force-deformation (if-d) relationship. The if-d function used to depict the collision could be theoretical or empirical, depending on the state of knowledge regarding the force-deflection capabilities of the bumpers. The system's rebound characteristics are used in an if-then-else statement to account for bumper rebound during a simulated collision. Acceleration versus time data for all simulated vehicles can be obtained using a numerical simulation model. Dynamic if-d curves were calculated for three separate experiments involving low-velocity collisions. To verify the analytical model's ability to effectively characterize the vehicle dynamics in a previous incident, three low-velocity collision tests were redone. The model is used for parametric testing to explain the relationship between the bumper's structural characteristics and the closing speed and the crash pulse, and it is also used to identify the most severe low-speed collision ever recorded [30].

This study focuses on how to determine which geometric bumper beam concept is most suited to meet product safety requirements (PDS). The hybrid composite was compared to bumper beam designs with the same frontal curvature, thickness, and dimensions. Abaqus V16R9 performed an equivalent low-velocity impact test. Six factors—deflection, strain energy, mass, cost, ease of production, and ribs' potential—were equally important. The algorithm Topsis was used to determine whether theory was more superior. This study's results lend support to the hypothesis that a double hat profile (DHP) fabricated from the necessary material model should be employed for a small car's bumper beam. Strengthening the chosen idea to meet the PD's requirements is possible through the addition of strengthened ribs or a thicker bumper beam [31].

Designed a bumper with minimal weight by using glass thermoplastic (GMT) components. This bumper absorbs impact energy by deformation or transfers it perpendicular to the path of impact. To achieve this objective, a mechanism is intended to convert approximately 80% of the kinetic impact energy into spring potential energy and release it into the environment at a low impact velocity, per American standard 1. In addition, the passengers will not feel the collision since the leftover kinetic energy will be dampened by the microscopic elastic deformation of the bumper parts. CATIA, ls-Dynamics, and Ansys v8.0 were used to model, solve, and analyze the results, respectively. But the GMT cone-shaped part of the bumper was made to absorb as much of the impactor's speed as possible in high-speed collisions [32].

In this research, we show that a stress study performed with a BEM sub-model greatly improved upon previously proposed modifications to the bumper's fascia. Automobile parts typically fail as a result of stress concentration; however, this problem may be solvable with the help of numerical analysis. In this case, the boundary element method (BEM) is adapted from its original purpose in stress analysis to aid in the manufacturing of a car part. The finite element technique (FEM), used in the automobile sector for stress analysis, yielded similar findings [33].

In this paper, important circumstance in vehicle design, we built and refined the crashworthiness of a bumper subsystem. In order to solve the bumper design problem, a unified method for multi-attribute design engineering of mechanical structures was developed. The various manual processes are captured by the integrated procedure, which makes the automated design iterations needed for improvement much easier. Finally, an optimization technique is carried out to account for the impact of parametric uncertainties in a way that yields a satisfactory system failure probability. Possibility-based design optimization is an approach for maximizing a system's potential that makes use of crash simulations' fuzzy FE analysis to account for, and mitigate, unpredictability. This strategy is analogous to statistically defined parameter reliability-based design optimization (variabilities) [34].

In this paper, examined the brackets that were holding the vehicle's hollow beams in place. The automobile is traveling at 50 km/h and hits the wall at a 40 degree angle. To make the beam safer in the event of a collision, they worked to boost its ability to soak up impact energy. Using an explicit finite element method, we were able to reproduce the collision's occurrence. The shape of the beam's cross-section is a function of the design variables. The beam was optimized with a hybrid search strategy that combines genetic and nelder & mead algorithms. According to the data, the bumper beams' resilience in a collision has been much enhanced. The optimal shape was sensitive to the precise nature of the target function, the number of design variables, and the scope of the feasible design space. When compared to the two best alternatives found in this research, the currently utilized form is significantly inferior [35].

In this work, investigated the impact properties of automobile bumpers. In order to model a crash, scientists have developed a theory for using explicit nonlinear finite elements. Finite element analysis of a low-velocity collision between a car bumper system and a pendulum was carried out in accordance with ece-r42. HyperView was used to conduct an objective and comprehensive analysis of the stress and strain contours, node displacement on the deformation zones of the bumper beam, crash box compression, and energy conversion process. There was additional research into how factors like bumper beam thickness, section shape, and material quality affected crash characteristics. The results showed that the beam's initial energy value per unit mass absorbed could be improved by decreasing the beam's thickness, and that the cross-sectional shape had a limited influence on the crash performance. Therefore, increasing the beam's thickness was unnecessary. The use of aluminum alloy not only improved the bumper's crash performance but also reduced its weight. Analysis of the frontal collision bumper beam Aluminum honeycomb bumpers were a considerable reason why sandwich panel structures with low strength-to-weight ratios could not be used [36].

In this work, I looked at several bumper beam shapes to find one with the highest possible impact resistance. To replicate the collision consequences seen in real-world testing, we drove a vehicle at 64 kilometers per hour into a deformable barrier that was offset by 40%. The bumper beam and the brackets that hold it up are modeled as deformable entities with a high degree of physical detail. We build a lumped parameter model for the remaining auto parts. The impact scenario is modeled using an explicit finite element approach. To find the best beam configuration, a search strategy that combines genetic algorithms with nelder-mead methods is employed. Evidence from this study showed that the present bumper beam's crashworthiness was significantly enhanced. The system's resilience to low-velocity impacts was also improved. Specific strain energy absorption is improved by 16% in the perfect beam compared to the best form currently in use. Furthermore, the low-speed crash resistance was significantly improved [37].

In this paper, Researched and modelled an automobile bumper to be used in a low-velocity impact test to enhance its crashworthiness. In order to understand how aluminum and composite materials react to impact, a crash test was conducted on the bumper. It was found that materials with a low young's modulus had a correspondingly low rigidity, however those with a high strength produced good impact behavior, as the yield stress was always higher than the bumper's maximum stress. For these uses, aluminum has always been the best metal to go with. Perhaps increasing the bumper's thickness might help increase its impact force and rigidity. Also, ribs added to the bumper might make it stiffer, which would raise the impact force and decrease the bumper's deflection. However, manufacturing bumpers with ribs is challenging for manufacturers. When considering a replacement for GMT, SMC Composite was proposed as a superior option due to its many advantages over GMT, including its low cost and eases of production. In order to lessen deflections, the ribs in the bumper construction were removed. SMC composites, which showed maximum stress values, were likewise stable at higher speeds [38].

In this paper, to better understand the physical processes at play during off-center hits of a longitudinal automotive bumper beam system, this study was carried out to verify a modeling method. Simulating the forming process allowed for the creation of a FE model of the bumper beam with the appropriate curvature. We used the finite element (FE) code Ls - dyna to compare how well different materials in a bumper beam fared under asymmetrical impact loads and to provide a material recommendation. In order to study the bumper beam member's dynamic behavior, a number of variations on the materials and structural features were tested. With the help of the quality requirements, the bumper beam member was modeled in the FE code Ansys-dyna to get the best result possible. The following analysis yielded these findings: The aa7003-t79 has a greater plastic flow and is stiffer than the aa7003-t1 and the aa6060. If you compare aa7003-t79 to aa6060-t1 and aa7003, you'll see that it deforms by just 3% and 2.4%, respectively, with the necessary impact force. The aa7003-t79 bumper distributes less energy to passengers than the aa6060-t1 bumper (by 5%) and the aa7003 bumper (by 15%). Traveler acceleration is reduced using aa7003-t79 bumper beams [39].

The bumper beam technology employs FGF-filled beams to absorb additional force. The explicit finite element technique, ls-dyna, proved best for generating a numerical FGF-filled bumper beam model. A parametric model tested bumper beams packed with FGF and UF for impact resistance. FGF-filled bumper beams absorbed impact energy better than UF-filled ones of the same weight. Finally, a validated passenger car model was hit by a frontal rigid wall at 50 km/h and an offset ODB impact at 64 km/h to compare the knee-area bumper beam solutions of UF and FGF. FGF-filled bumper beams were 14% lighter than regular bumper beams and provided the same impact protection in simulations [40].

This study presents a system of bumpers that absorbs some of the impact energy within a small space between the bumper's back face and the vehicle's body components. The goal of the paper was to demonstrate the potential of finite element analysis software for simulation throughout the vehicle design process. Here, we analyze the international safety standards using a stiff wall impact on a variety of materials. Some of the finite element applications utilized here include Hyper mesh, Radios, Hyper View, St. inspire, and Hypergraph. The results demonstrate that for every one kilogram that is cut from the weight of the bumper beam, the first base design's displacement increases by up to five millimeters in the third, better design. Because of its lower weight and higher resistance to impact loads, carbon fiber composite material has been chosen as the optimal material for bumper beams. Bumper beams, then, need to be fabricated from a carbon fiber composite [41].

The researchers in this study modelled low-velocity impacts on a bumper beam's material, shape, and deformation to improve crashworthiness. Maximum deflection studies bumper beam elastic mode strength in relation to impact force and absorbed energy. To find the best bumper beam material, computer simulations investigated deflection, stress distribution, impact force, and energy absorption. M220 reduces bumper beam deflection, impact force, and stress distribution while increasing elastic strain energy, according to research. Passengers changed accident dynamics. We could track changes in calculated parameters over time. Two main factors were considered while developing the bumper beam. Bumper beams absorb impact energy better when made of high-yield strength, modulus-elastic material. Second, the bumper beam shouldn't distort plastically at low velocity. Bump beam distortion was below the maximum allowed. [42].

In this study, we present a bumper, crash box, and front rail assembly that is lighter and more crashworthy than previous designs thanks to structural optimization and the use of high strength and high mass efficiency replacement materials. Collision box, Aluminum 6060, trip800, and dp800 were used in the construction of the new bumper and front rail. Aluminum foam was substituted for the bumper's original strengthened plate, which greatly increased the crash box's efficacy. One thing's worth was weighed against a hypothetically perfect set of interchangeable but equivalent alternatives. We used an elite strategy genetic algorithm and a reaction surface surrogate model to numerically simulate the lowest mass that met crashworthiness requirements. Energy absorption, peak impact force, crumple distance, and overall mass may all be improved by 11% if just one material could be optimized. Even better outcomes resulted after further iterations of form and function refinement. Foam-filled bumpers work along with the crash box to absorb more energy, reducing the negative effects of bumper mid-bending, which causes bumper failure of load bearing. Increasing crash resistance and reducing weight using many materials in a single design may be possible with the use of a hybrid approach [43].

This work used nonlinear FE computations to expose vehicle bumper structural models to full-scale impact stresses. Construction uses cattails and bamboo. According to the research, bionic bumpers absorb greater impact (sea). The bionic bumper's bionic cross - beam and box improve crashworthiness, according to numerical analysis. Bionic cross - beams had 33.33 percent less crush deformation and 44.41 percent less weight than box bumpers. Because it dissipates impact force, bionic bumper bodies are perfect for the future. Using ls-dyna, this research crashes three FE models. Bionic bumpers statistically reduced crash safety. The bionic bumper models absorbed energy better than traditional ones [3].

In this paper, the impacts of the low-velocity collision test mandated by the IIHS were analyzed from three different perspectives: from the right, from the left, and from the vehicle's center. Using fine element analysis (FEA), designers may examine variables like bumper material, shape, thickness, and impact condition to determine how to best improve crashworthiness in low-speed impacts. In order to counteract this, the vehicle's front end was altered. Aligning the front metal bumper with the appropriate rigidity has been demonstrated to yield the greatest results, which in turn prevents damage to automotive components. All four variations demonstrate the importance of the metal front bumper and crush bracket in absorbing impact energy at low to medium speeds. The new metal bumper has an energy-absorbing capability that is roughly a factor of 1.3 higher than the previous design. When two automobiles collide at moderate speeds, it has been noticed that their bumpers match geometrically, leading to contact. Crash energy management systems have been seen to benefit most from bumper thickness, number of crush initiators, form, and profile [44].

Developed a front bumper self-adjusting modular energy absorber to address these issues. The x-shaped energy-absorbing structure was designed to enhance impact energy absorption by adapting its mode of deformation to external collision energy. A real automobile bumper system outperforms a foam energy absorber in finite element simulations of crashworthiness. A thorough factorial method examines the structural properties of the x-shaped energy-absorbing, and multi-objective optimization is done for pedestrian safety and low-speed impact assessment indices. Variables include thickness, lateral arc radius, and clamping boost beam thickness. After optimizing, we prove our aims are achievable. Finally, by altering key deformation modes in response to impact energy, the innovative x-shaped energy absorber meets pedestrian safety and low-speed impact standards. We use multi-objective structural parameter optimization for the innovative energy absorber. The new energy absorber's structural changes have improved pedestrian safety and reduced low-velocity accidents. It increases pedestrian safety and reduces low-impact collisions [11].

To examine stress absorption, researchers vertically broke bionic bamboo tubes (BBTs) in 2019. Bamboo's unique cellular structure inspired six tube cross-sectional designs. We examined rib form and count changes using the finite element tool ls-dyna. Researchers revealed that "x"-shaped and six-rib BBT designs were the most crash-resistant. For optimal energy absorption, these BBT structures' rib angle, center distance, and thickness were tuned using multi-objective optimization. RSM+MOPSO increased SEA and decreased peak crushing force (PCF). The improved BBT structure enhanced sea value by 6.84% while maintaining its maximum crushing force. The new BBT will be more collision-resistant if the center distance (24.61 mm), rib angle (39.50 °), and rib thickness (0.50 mm) are followed. SEA and PCF climbed, but SEA increased more (6.84 vs. 0.72) [45].

Examined the shape geometry to design a suitable structure for a bumper, and then assessed its impact behavior to find out how much energy it could absorb. Simplicity in production was also studied at the same time. We compared the dynamic behavior of the upgraded front bumper with and without a stiffener by simulating an impact on both versions of the bumper. It was determined that the bumper with the stiffener had a greater capacity to absorb energy. The natural frequencies obtained from an FFT analyzer were experimentally verified using modal analysis with finite element analysis software, and the results were quite similar. While developing the prototype, we discovered that the expected bumper structure could be simply made. Research into impact dynamics has shown that bumpers that are both well-shaped and have a stiffener are the most effective. [46].

2.3 CONCLUDING REMARKS:

The majority of the literature review's authors focused on the enhancement characteristics of mechanical properties and impact resistance.as well as considering the redesign that guarantees light weight and enhancing the ratio of absorbed energy.

However, many researchers have focused their work on the following:

a. The front impact absorber system for cars was designed in brackets of 5 miles per hour and the LS-DYNA codes nonlinear dynamic contact analysis was used for the simulation.

b. LS-DYNA, a commercial explicit FE code, was used to evaluate the school bus model to simulate accidents with full-scale FE vehicle models used as bullet vehicles.

c. Improving the impact resistance at low velocity and adjusting the front bumper structure of the car accordingly.

d. Using LS-DYNA for impact modeling and evaluating the front bumper made of glass thermoplastics and comparing it with conventional metals such as steel and aluminum, as well as the LS-DYNA was able to provide very accurate predictions of the breakdown situation observed in experimental tests.

e. Investigates the impact and moment behaviors of aluminum by bending square girders packed with foam and gaps using finite element modeling.

f. Designing a bumper made of epoxy material reinforced with fibers, using an impact absorber to control the amount of material, and knowing the improvements that took place in the mechanical properties in the event of a collision.

g. Simulation of the bumper's design while the automobile is traveling 5 mph against a stiff wall led to design changes that reduced the shock absorber's weight.

h. Examine the radiation system filled with (FGF) to increase energy absorption upon collision using the LS-DYNA software in standard analysis, as well as studying the modeling and analysis of the automobile bumper to improve crash resistance in various speed tests.

i. A change in the structural characteristics of the bumper beam using the shape of cattail and bamboo plants, where the design inspired by nature improves the energy absorption and resistance of the structure to collapse and lowers the value of deformation, and it was better in absorbing energy than the original type.

j. The X-shaped design of the energy-absorbing structure allows for fine-tuning of the mode of deformation during usage, resulting in a greater energy-absorbing capacity overall.

k. Some of these steps include alterations to the structure, such as the installation of aluminum foam to absorb shocks and the addition of reinforcements to the original materials to strengthen their strength in the face of impact. Energy absorption was improved by replacing the site's original reinforced plate.

l. Numerical results from our study of the energy-absorbing characteristics of bamboo tubes in six different cross-sectional configurations based on bamboo's micro-structure are analyzed in the LS-DYNA software.

m. Shape geometry analysis to build the optimal structure. The observatory was conducted, and an impact behavior analysis was conducted to determine its ability to absorb energy. Indicator Models for Impact Safety is the strongest and shape-optimal design for energy dissipation.

3. EXPERIMENTAL AND NUMERICAL PROCEDURE

3.1 CONSEQUENCES OF VEHICLE ACCIDENTS

It is well known that, like other types of collisions, those involving fast-moving cars happen in a very little period. In the first place, the need to change momentum mv leads to a dominant average force (F) over time t and the emergence of surfaces of impact; F is inversely proportional to (t), or **F = mv/t**. so, the greater the force (F), the shorter the duration (t). Those inside the car(s) who aren't wearing seatbelts will feel a lot of acceleration (or deceleration) when the car(s) hits anything solid, especially their heads. For an example of a common head collision, see Figure (3-1).

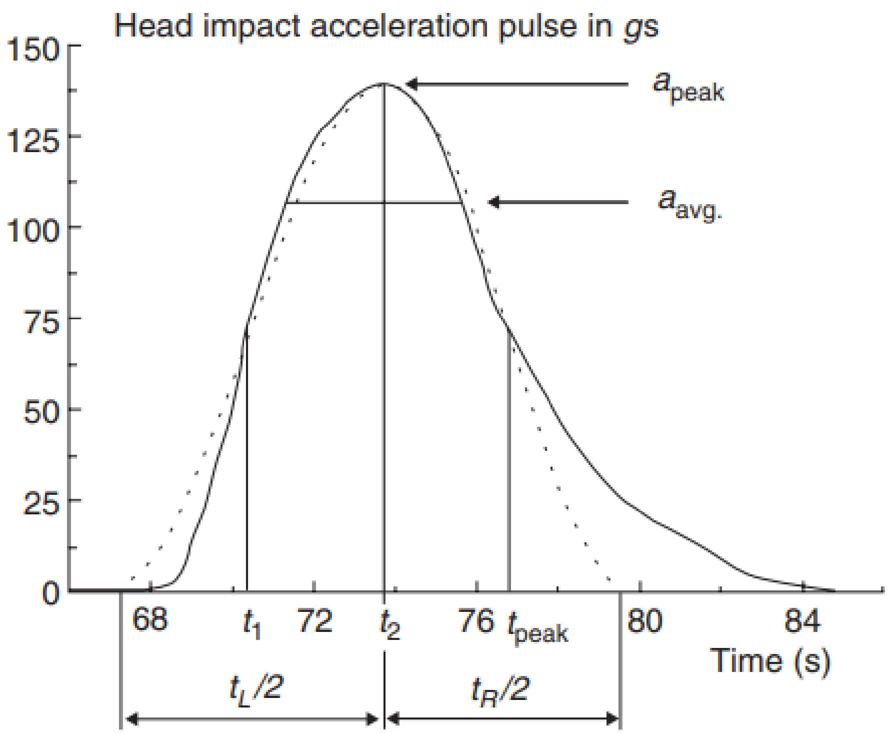

Figure 3.1: Acceleration pulse typical of a car accident test (reprinted with permission of Global Academic Publishing).

Pulse of acceleration: a fast, brief (3–25 MS, typically) powerful impact with rapid loading and unloading. Serious harm to people and structures may result from this strong force or acceleration [47]. the outcomes of a vehicle collision may be broadly described as follows:

a. The impact resulted in plastic distortion and fracture of the vehicle's structure in addition to its destruction by fire.

b. Damage to humans (or sometimes other living beings like animals), which refers to bodily and/or mental pain and stress to the individuals inside the vehicle and/or outside the vehicle (trees, poles, guard rails, etc.), it is important to note that in a crash involving a sudden deceleration, the occupants' heads may collide with interior features such as side rails, pillars, the roof, or the windshield. The second impact is what this is known as, and it might potentially be quite hazardous.

3.2 APPLICATIONS OF MATERIALS AND STRUCTURES OF ENERGY-ABSORBING

The public is more informed and vociferous than ever before, calling for stricter legal repercussions for technological mishaps and higher standards of personal and public safety. Due to these factors, it is crucial to have up-to-date understanding of passive safety measure design in order to apply them in this sector. Energy-absorbing structures and materials, which can transfer kinetic energy upon impact or severe dynamic loading, have been the focus of scientific and engineering study and development since the 1970s. The automotive and defense sectors can attest to this [48], [49]. The following are summaries of their main uses in five categories.

3.2.1 Structures In Automobiles That Absorb Impact Energy To Make Them Safer In Accidents

Safety in collisions is an important yet challenging aspect of vehicle design and testing. Safety in a crash, or crashworthiness, is how well a car handles itself in a collision. The stronger the crashworthiness or crashworthy performance of a vehicle, the less damage will occur to the vehicle, its occupants, and/or its cargo after a given occurrence [47]. Figure (3-2) depicts several popular terms used to describe automobile body structures. Cars typically have steel columns with thin walls for their body frames. After an accident, the upper and lower rails at the front of a vehicle's body are the principal energy-absorbing structures. Front and rear bumpers may contribute to minimal frontal and lateral impacts when a car slams into a tree or utility pole at low speeds, as may occur in a parking lot [50], [51]. In the event of a collision, the passenger compartment is designed to be protected by the B-pillar, A-pillar and roof side rails (see Figure (3-2)). However, in the event of a quick deceleration, they could become impact zones for the occupant's head. Since the head is in touch with the sheet metal of the column, it seems unlikely that the required force can be met (see below). The column needs an extra pad to act as a shock absorber [52].

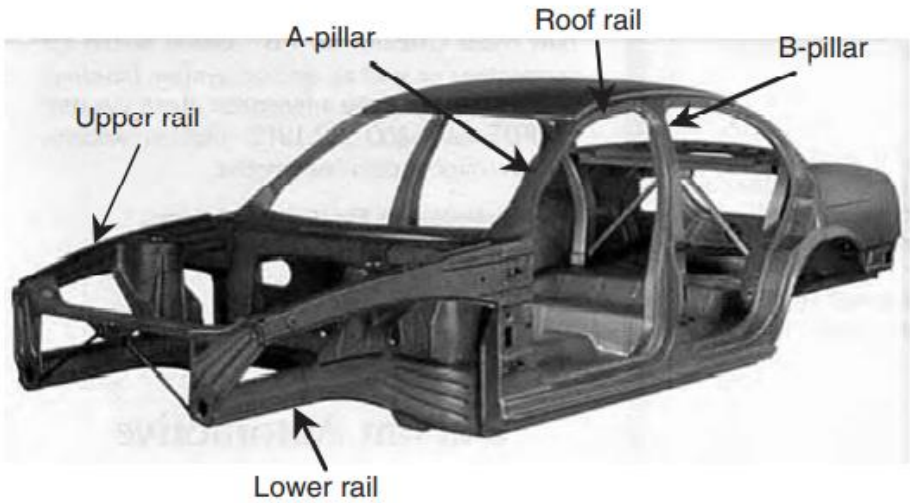

Figure 3.2: A body structure for a car (With the consent of World Academic Publishing).

When heavy traffic flows traverse a complex road system, side impact protection for the driver or passengers (which accounts for approximately 13% of all serious automobile injuries) has become critical, while frontal and rear-end collisions remain the most serious. In the zone of impact for many automobiles, there is minimal room for an entry before a human body is confronted, which poses a unique difficulty. Several manufacturers have incorporated reinforced doors and sturdy supports that can sustain a 50 km/h collision, allowing for a minimal breach of the "safety cell" surrounding the driver and passengers. New designs have also enabled seats, steering wheel systems, and other structural components within cars to have a particular energy absorption capability, thus enhancing the total energy absorption of vehicles during collisions.

3.3 CHARACTERISTICS OF ENERGY-ABSORBING BUILDINGS IN GENERAL

Under operating pressures, most structures (including those utilized in civil engineering and equipment) only show little elastoplastic deformation. A significant consideration in deciding the materials used and the design decisions made is the elastic stress or strain that a structure must bear. Long-term usage usually results in breakdowns due to fatigue, corrosion, or material degradation. By contrast, the design and analysis of energy-absorbing structures deviates significantly from the standard in structural engineering. The large impact loads that energy-absorbing structures must withstand need complicated interactions between deformation modes including bending and stretching as well as strain hardening and strain rate effects to prevent the structure's premature collapse. For these reasons, ductile materials are typically used for energy absorbers. Polymer foams and polymers with fibers in them are common examples of non-metallic materials utilized when saving weight is paramount. The research of energy-absorbing structures often begins with quasi-static analysis and testing. Different types of deformation seem to react differently to dynamic stimuli, which make it hard to measure deformation and failure with scale model testing, according to several studies. It is there that we will address the need for further in-depth scientific study of crashworthiness and impact protection, both of which are well-defined challenges. Engineering plasticity is an established field that will be used to assess and forecast the effectiveness of energy-absorbing structures fabricated from ductile materials. So, unlike traditional structural analysis, which aims to optimize a building's structural integrity, research into energy-absorbing structures has a distinct ultimate purpose. Ideas in General It is clear from a discussion of the development of engineering for energy-absorbing structures that the design and selection of energy-absorbing materials must be tailored to each structure and the specific conditions under which it will operate. While the designs and materials employed for various purposes may differ greatly, they nonetheless share a common goal: the uniform and predictable distribution of kinetic energy. As a result, certain notions may be utilized as benchmarks across fields. The most vital ones are these. Stop the energy flow indefinitely and invert it the kinetic energy must be dissipated or permanently transformed into an inelastic form, such as by plastic deformation, rather than stored elastically in the structures or materials. To what end must it be so rigid? When a protective structure is stretched to its limit, the elastic strain energy it received from the original kinetic energy (or, more generally, the input energy due to dynamic loading) is released, harming both the person being protected and the protective structure. Visualize a high-speed automobile crash with a massive elastic spring. In the first stage, the vehicle's initial kinetic energy is transformed into the spring's elastic strain energy as the spring is elastically compressed and the car slows down. Maximum elastic displacement is reached when the spring begins to slowly return to its original shape, at which point the vehicle begins to speed up (Figure 3-3) and all of the elastic strain energy is transformed back into kinetic energy. Thus, the passengers will feel a sudden and harsh deceleration followed by a rapid acceleration. Since the severity of an accident rises in direct proportion to the rate of acceleration and deceleration, this might have disastrous effects for the people within the car. Multiple forms of irreversible energy, including viscous deformation energy, plastic dissipation, and energy lost due to fracture or friction; occur throughout the massive deformation process of structures and materials. It's possible that some of them are related.

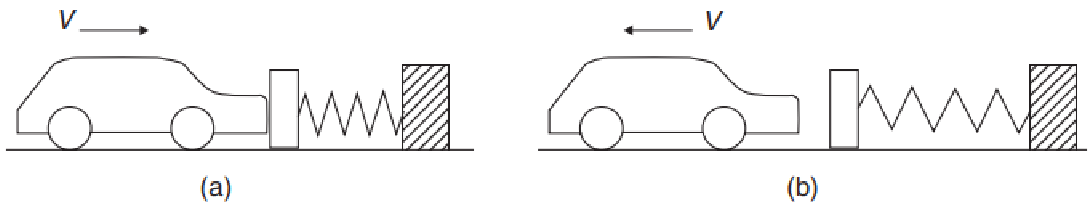

Figure 3.3: A automobile collides with an elastic spring: (a) it is decelerated by the compression of the spring. (b) it is reaccelerated by the spring's recovery.

Some cracks and deformations are due to actions on a meso- or micro-scale, whereas others are due to processes at a macroscopic size. For example, macroscopic inter-laminar fractures, viscous deformation of the matrix, micro-cracks at fiber/matrix contacts, and internal friction in fractured materials are all common contributors to delamination in polymer-matrix laminate composites. Among ductile materials (metals and polymers), this is the most efficient way for absorbing energy and offers the widest range of applications. Constantly constricting reactive forces as the energy-absorbing structure deforms slowly over time, it's important that the peak response force stays below a certain threshold. The reactive force must remain constant or nearly constant to avoid an unacceptable high rate of retardation, and the peak force (and subsequently peak deceleration) of energy-absorbing structures and materials upon contact must be maintained below the level that would cause damage or injury. During a collision, a person's acceleration matches that of the vehicle when they are restrained by a seat belt. If the acceleration a(t) of the collision process does not change, we have a minimum. In other words, for safety reasons, it's important that the impact force between the colliding structures remains stable. In this technique, energy absorbers function as a specialized kind of load limiter; the most effective of them have a rectangular force-displacement curve.

3.4 MECHANICAL PROPERTIES OF MATERIALS IN TENSION

The most common and straightforward method for assessing the deformation behavior of a material in response to applied stresses is to perform a basic tensile test on cylindrical or flat samples of the material. Several technological substrates are suitable for this straightforward tensile test. The stress-strain diagrams for mild steel (a), aluminum alloy (b), and a knitted textile composite (c) are shown in Figure (3-4). For the most part, engineered materials undergo elastic deformation when subjected to even a little tensile tension, as shown in Figure (3-4). A material's linear elastic stage is described by two material constants: Young's modulus E, which defines the constant slope of the stress-strain curve, and Poisson's ratio n, which discloses the ratio of the negative transverse strain to the longitudinal tensile strain. Metals and polymers, for example, have yield points, or levels of stress at which they begin to crack or break. This not only signals a departure from the linear stress-strain curve but also the start of irreversible plastic deformation. Since the yield stress Y is a constant, as shown in Figure (3-4a), mild steel continuously deforms under normal conditions (also indicated by Sy in some books). However, for most materials, the necessary stress will grow as the deformation progresses. This phenomenon is called strain hardening. There are materials for which a linear or power law approximation of the stress-strain relationship is valid, as shown in Figure (3-4b).

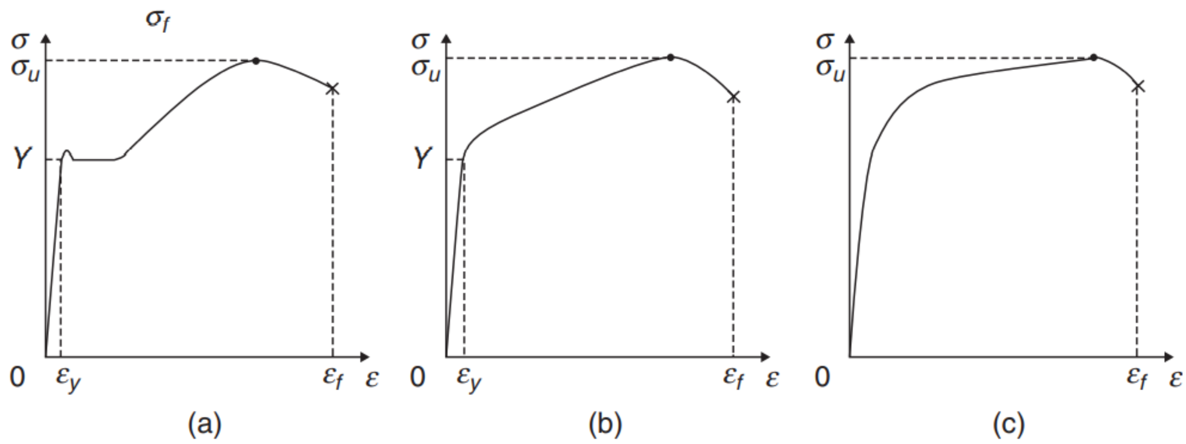

Figure 3.4: The following are the stress-strain curves for three different materials when subjected to tension: (a) the mild of steel, (b) aluminum alloy, and (c) knitted textile composite.

The plastic deformation step concludes when the material sample breaks under stress. Prior to fracture, the stress reaches its maximum, represented by the ultimate stress Su. The strain associated with a fracture is known as the fracture strain, represented by ef. These two numbers (refer to Figure (3-4a)) represent the material's tensile strength and ductility, respectively. Most engineering materials behave similarly under simple compression or pure shear as they do under tension, but the fundamental constants of the materials may be different.

3.5 MODELS OF IDEAL MATERIALS

It is required to idealize the mechanical behavior of the materials so that the stress-strain relationship can be characterized using basic analytical functions before developing relatively straightforward theoretical models for assessing the energy-absorption capacities of materials and structures. To simulate linear elastic materials, we utilize the Young's modulus E and the Poisson ratio n when the strain is small. As can be shown in Figure, once yielding has occurred, an elastic, totally plastic material model may be applied provided strain hardening is small (3-5a). In this context, the phrase "perfect plastic" suggests that strain-hardening is insignificant; that is, the material will continue to deform plastically from first yielding to fracture while the stress remains Y. Depending on how the material actually acts, as measured by its basic tensile test, either an elastic, linear hardening model Figure (3-5b) or an elastic, power hardening model Figure (3-5c) could be used if the strain-hardening after the first yield is large.

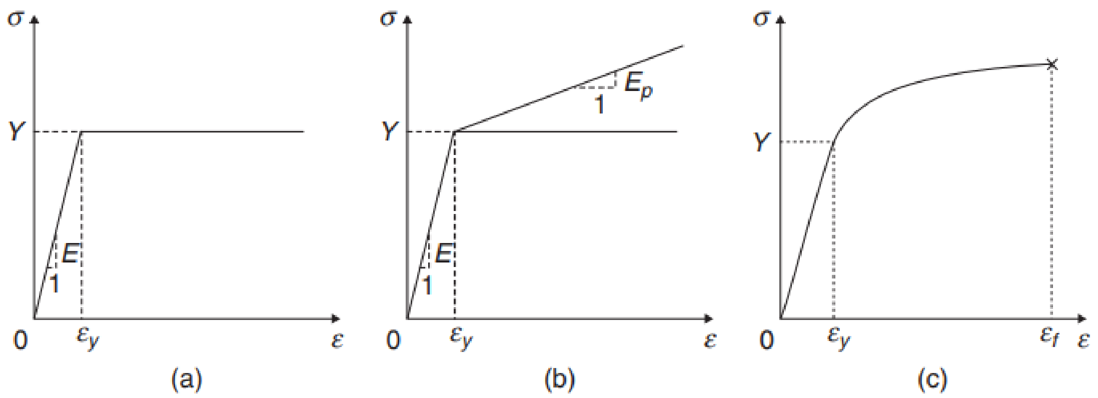

2.2

Figure 3.5: Tension-applied materials with idealized stress-strain diagrams: (a) perfectly plastic and elastic (b) linear hardening and elastic, (c) power hardening and elastic. Analytical expressions for the idealized connection between stress s and strain e are given below, which correspond to the models in Figure (3-5), (a), (b), and (c).

$$\sigma = \begin{cases} E\varepsilon & \text{for} \quad \varepsilon \le \varepsilon_y = Y/E \\ Y & \text{for} \quad \varepsilon_y \le \varepsilon < \varepsilon_f \end{cases} \qquad \dots (3.1)$$

$$\sigma = \begin{cases} E\varepsilon & \text{for} \quad \varepsilon \le \varepsilon_y = Y/E \\ Y + E_p(\varepsilon - \varepsilon_y) & \text{for} \quad \varepsilon_y \le \varepsilon < \varepsilon_f \end{cases} \qquad \dots (3.2)$$

and

$$\sigma = \begin{cases} E\varepsilon & \text{for} \quad \varepsilon \le \varepsilon_y = Y/E \\ Y + K(\varepsilon - \varepsilon_y)^q & \text{for} \quad \varepsilon_y \le \varepsilon < \varepsilon_f \end{cases} \qquad \dots (3.3)$$

where ey represents the yield strain, Ep the hardening modulus, K the material constant, and q the hardening exponent. The power-hardening model reduces to the linear-hardening model with the conditions q = 1 and K = Ep. The materials work well when used to soak up shocks. There will be situations where the plastic strain outweighs the elastic strain, prompting researchers to disregard the latter. Because of this, it is possible to assume that the material is completely rigid before the onset of yielding by treating Young's modulus as infinite. The simplified model of materials is sometimes called a rigid-plastic model to reflect this distinction. Rigid, totally plastic, rigid, linear hardening, and rigid, power hardening models are shown in (a), (b), and (c), respectively, in Figures (3-5).

3.6 BEAMS RELATIONSHIP OF MOMENT TO CURVATURE FOR PLASTIC BEAM

Elastic-plastic beams (or other 1-dimensional structural components like rings and arches) have a linear connection between the applied bending moment M and the curvature k of their central axis when M is modest (M Me, where Me is the maximum elastic bending moment). Integrating the correct s-e relation over the beam's thickness can help one arrive at the true M-k relationship. The stress distribution throughout the thickness of elastic, totally flexible beam with a rectangular cross section (or any 1-dimensional structural feature, such a ring or an arch) is depicted in Figure (3-6a), and it consists of an elastic "core" sandwiched between two plastic deformation zones. So, we may write the connection between the moment and the curvature as [53]

$$\frac{M}{M_e} = \begin{cases} \dfrac{\kappa}{\kappa_e} & \text{for} \quad 0 \le M \le M_e \\ \dfrac{3}{2} - \dfrac{1}{2}\left(\dfrac{\kappa_e}{\kappa}\right)^2 & \text{for} \quad M_e < M < M_p \end{cases} \qquad \ldots (3.4)$$

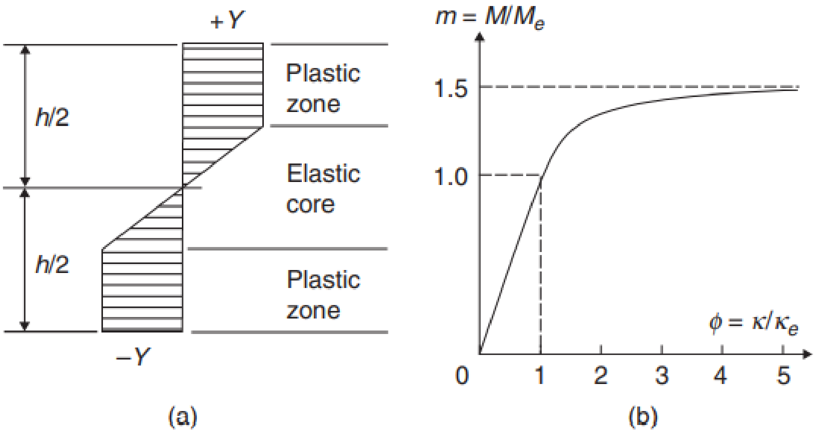

Figure 3.6: An elastic and perfectly plastic beam has the following properties when bent: (a) a uniform stress distribution across the beam's thickness; and (b) no dimensional moment-curvature connection.

Mp = Ybh2 /4 is the totally plastic bending moment of a beam with a rectangular cross-section, where b and h are the width and thickness, respectively; Me = Ybh2 /6 is the value of the maximum bending moment; ke = Me /EI = Me / (Ebh3 /12) = 2Y/Eh is still the value of the maximum curvature. The equation (3.5) may be expressed without the units of

$$\phi = \begin{cases} m & \text{for} \quad 0 \le m \le 1 \\ \dfrac{1}{\sqrt{3-2m}} & \text{for} \quad 1 \le m < \dfrac{3}{2} \end{cases} \qquad \ldots (3.5)$$

where the bending moment, m, is represented by the ratio M/Me and the curvature, f, is represented by the ratio k/ke, both of which are scalar quantities. A diagram of this connection is shown in Figure (3-6b). If the beam's cross-section has a non-zero curvature, the stress profile along the beam's thickness will only contain plastic zones if a stiff, fully plastic relation between stress and strain is used, as illustrated in Figure (3-5a) (3-7a). Accordingly, as can be seen in Figure, the relationship between bending moment and curvature is written as a step function (3-7b).

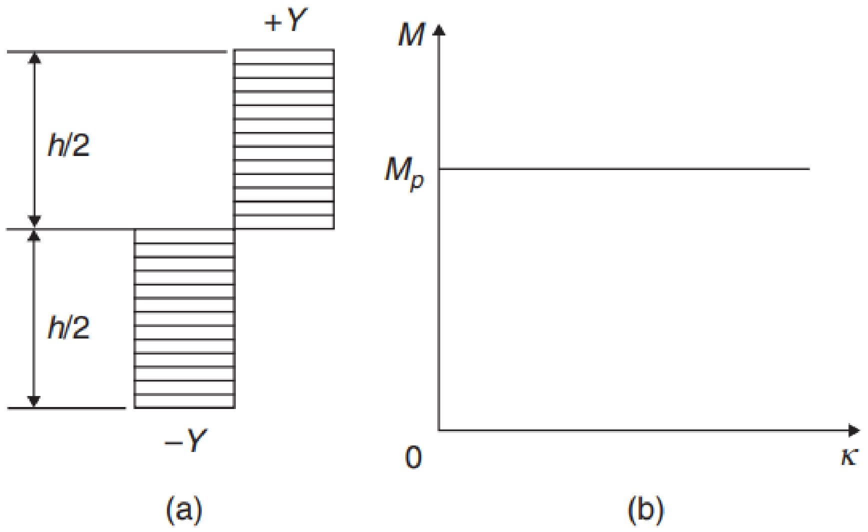

Figure 3.7: The stress distribution over the thickness of a completely flexible, stiff beam during bending (a) and the relationship between moment and curvature (b).

$$\begin{cases} M \le M_p & \text{for} \quad \kappa = 0 \\ M = M_p & \text{for} \quad \kappa > 0 \end{cases} \qquad \dots (3.6)$$

3.7 PLASTICITY THEORY

Plastic deformation occurs when an item is subjected to an external load that exceeds its maximum elastic yield stress, and the distortion is irreversible/permanent. If the deformation recovers its previous form, it is referred to as elastic deformation. [54]

Plasticity is the study of the stress-strain and load-deflection relationships between ductile materials or plastically deformed structures. Experimental observation and mathematical representation should be used to establish such relationships.

In general, the stress situations that arise during an experiment are simple and uniform. Still, the end goal of every theory of plasticity is to come up with a general mathematical formula that can predict plastic deformation under complicated loading and boundary conditions. [54]

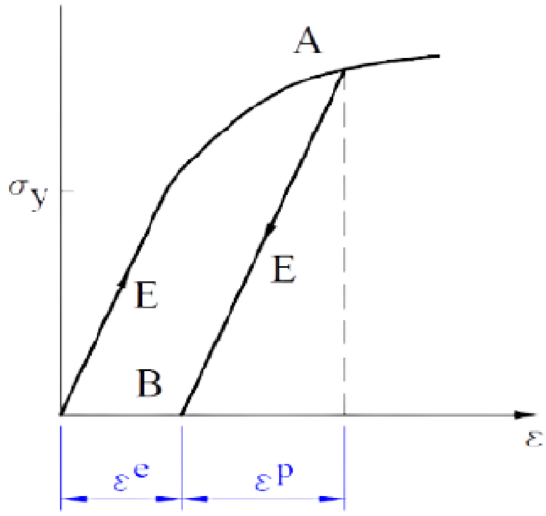

Figure 3.8: $\sigma - \varepsilon$ the curve for a plastic-elastic material [55]

The material is linear until the yield point σy, after which plastic deformation begins at εp (plastic strain) as illustrated in Figure (3-8).

In the elastic area phase (before to the yield point σy), the removal of a load allows the deformed material to revert to its original shape. However, when a bigger load is applied that exceeds the yielding point and enters the plastic zone, the material is plastically deformed and will not return to its original shape even when the load is removed. As seen in the figure, there is a recovery upon unloading at point A. At point A, the total stress is the sum of the plastic strain ε^p and the elastic strain ε^e.

3.8 THE CRITERIA OF YIELDING

When the stress value on the stress line graph reaches the yield point, plastic yield occurs for an object under uniaxial tensile stress. But with triaxial stress, only one stress component isn't enough to determine the yield strength. A material's predicted yield status in a complex stress condition is based on a relationship between the stress components. Ductile materials must meet one of two major yield requirements. The authors are Von Mises and Tresca [56]

3.8.1 The Energy of Strain

Under stress, the object bends. Meanwhile, the object's body stores strain energy as a result of the force. In this case, the pressure energy contained in the item cannot be uniformly distributed. Therefore, the concept of "strain energy density" was put forward. What we call "energy density" (or "U0") is actually the strain energy per unit volume. Integration yields the total stress energy of a given object [56]

$$U = \iiint U_0\ (x, y, x) dv \tag{3.7}$$

Strain energy density is equal to the region under the stress energy curve for uniaxial stress. [56]

$$U_0 = \frac{1}{2}\, \sigma\varepsilon \tag{3.8}$$

Here is a standard three-dimensional expression for the strain energy density: [56]

$$U_0 = \frac{1}{2}\, [\sigma_x\varepsilon_x + \sigma_y\varepsilon_y + \sigma_z\varepsilon_z + \tau_{xy}\gamma_{xy} + \tau_{yz}\gamma_{yz} + \tau_{xz}\gamma_{xz}] \tag{3.9}$$

As long as the material is still in the elastic zone, the stress energy is released when the load is removed. If the primary stress directions are parallel to the coordinating system, and there are no shear components in the coordinating system, then Eq. (3.9) can be reduced as follows: [57]

$$U_0 = \frac{1}{2}\, [\sigma_1\varepsilon_1 + \sigma_2\varepsilon_2 + \sigma_3\varepsilon_3] \tag{3.10}$$

Stress and strain are related in an elastic region according to the General Hook rule:

$$\begin{cases} \varepsilon_1 = \dfrac{1}{E}\ (\sigma_1 - \vartheta\sigma_2 - \vartheta\sigma_3) \\ \varepsilon_2 = \dfrac{1}{E}\ (\sigma_2 - \vartheta\sigma_1 - \vartheta\sigma_3) \\ \varepsilon_3 = \dfrac{1}{E}\ (\sigma_3 - \vartheta\sigma_1 - \vartheta\sigma_2) \end{cases} \tag{3.11}$$

Principal stresses that may be used to describe the energy stress density are as follows:

$$U_0 = \frac{1}{2E}\, [\sigma_1^2 + \sigma_2^2 + \sigma_3^2 - 2\vartheta(\sigma_1\sigma_2 + \sigma_2\sigma_3 + \sigma_1\sigma_3)] \tag{3.12}$$

Energy density under strain may be broken down into two parts: expansion strain and distortion strain. The energy density of the strain caused by an expansion is proportional to the strain's volumetric expansion. The morphological change is caused by an increase in the energy density of the distortion strain [56].

3.8.2 Efforts to Distort Energy (Von mises)

According to von Mises, yield is reached when the strain energy density of a ductile material reaches a critical value. With the assumption that this holds true for uniaxial stress as well, the critical value of the distortion energy may be determined using a uniaxial stress test. As yielding begins during a uniaxial stress test, the stress is as follows: σ (1) = 〖σ〗 y, σ 2=0, σ 3=0. The energy density at the point of yield is stated as follows: [56]

$$U_d = \frac{1+\vartheta}{3E} \sigma_y^2 \tag{3.13}$$

The energy density provided by the preceding equation is the fundamental value of the material's energy density of distortion. Von Mises's yielding criterion says that a material starts to fail when the energy density of the deformation reaches a certain level under a multiaxial load [56]

$$\frac{1+\vartheta}{3E} \sigma_{VM}^2 \geq \frac{1+\vartheta}{3E} \sigma_y^2 \tag{3.14}$$

$$\sigma_{VM} \geq \sigma_y \tag{3.15}$$

According to the distortion energy hypothesis, a component's failure is caused by its distortion, not its volumetric changes. Mises' Eq (1.6) is used to calculate the stress. All stress components may be expressed as follows:

$$\sigma_{VM} = \sqrt{\frac{(\sigma_{xx} - \sigma_{yy})^2 + (\sigma_{yy} - \sigma_{zz})^2 + (\sigma_{zz} - \sigma_{xx})^2 + 6(\tau_{xy}^2 + \tau_{yz}^2 + \tau_{zx}^2)}{2}} \tag{3.16}$$

The following defines the Mises stress in the context of the major stresses:

$$\sigma_{VM} = \sqrt{\sigma_1^2 - \sigma_1 \sigma_2 + \sigma_2^2} \tag{3.17}$$

Using the standard stress components, we may represent the stress resulting from Mises in terms of the stress instance in a two-dimensional plane σ_3=0.

$$\sigma_{VM} = \sqrt{\sigma_{xx}^2 - \sigma_{xx}\,\sigma_{yy} + \sigma_{yy}^2 + 3\tau_{xy}^2} \tag{3.18}$$

Two-dimensional energy distortion equations σ1-σ2 also define a planar ellipse Figure 3 2. The inner portion of the ellipse indicates a biaxial stress zone in which static loading will not cause the material to yield.

If there were no normal stresses and just shear stresses, $\sigma_1 = -\sigma_2 = \tau =$ " and $\sigma_3 = 0$ would be the primary stresses. As seen in Figure (3-9), this pure shear on the σ_1-σ_2 plane is represented by a straight line passing through the origin at -45°. As illustrated in Figure 3 2, this line intersects von mises' ellipse at two places A and B. Equation (3.17) provides the amplitudes of the 1 and 2 stresses at these places

$$\sigma_y^2 = \sigma_1^2 - \sigma_1\,\sigma_1 + \sigma_1^2 = 3\sigma_1^2 = 3\tau_{max}^2 \tag{3.19}$$

$$\tau_{max} = \sigma_1 = \frac{\sigma_y}{\sqrt{3}} = 0.577\sigma_y \tag{3.20}$$

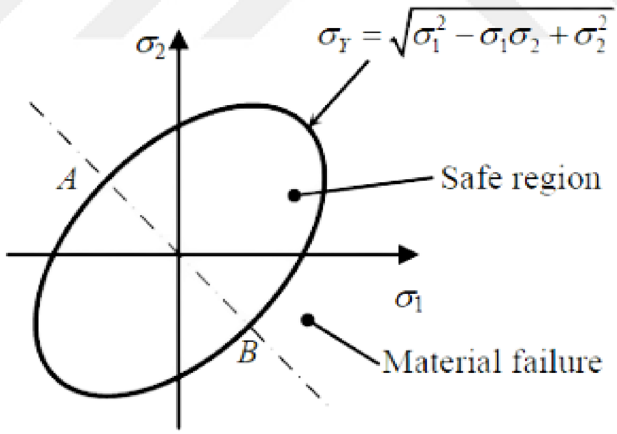

Figure 3.9: Geometric representation of energy theory of distortion.

3.9 STRAIN HARDENING

Experiments show that a solid's resistance to deformation is improved by subjecting it to loads that exceed its yielding force, discharging it completely, and then applying loads in the same direction for the return operation. Using this method, the product's yield strength may be increased. This is known as stress hardening, and it occurs often in metals. Figure (3-10) shows that the secondary yield occurs when the specimen is subjected to plastic stresses up to point B during the tensile test and again during the tensile test. Increases in yield strength due to stress hardening result in a greater separation of points A and B [58]

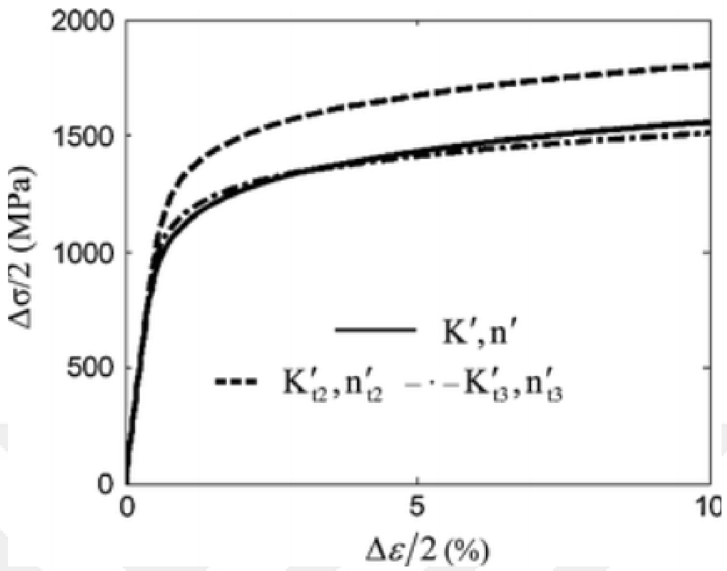

Figure 3.10: Yield stress due to strain hardening [59]

3.10 THE MODELS OF IDEAL MATERIAL

Since it is difficult to numerically characterize the materials' true stress behavior, various ideal material models have been used instead. This article provides introductory details on many popular models of perfect materials [60]

3.10.1 Kinematic Hardening Model

Bauschinger's effect adds complexity to any attempt to simulate the deformation of polymers. The kinematics hardness model, a reduced-complexity representation of the Bauschinger effect, has been proposed as a solution to this issue. Starting from the initial yield point, this model compares the reduction in return stress to the increase in stress experienced by a sample loaded in its original orientation above its yield stress [61]

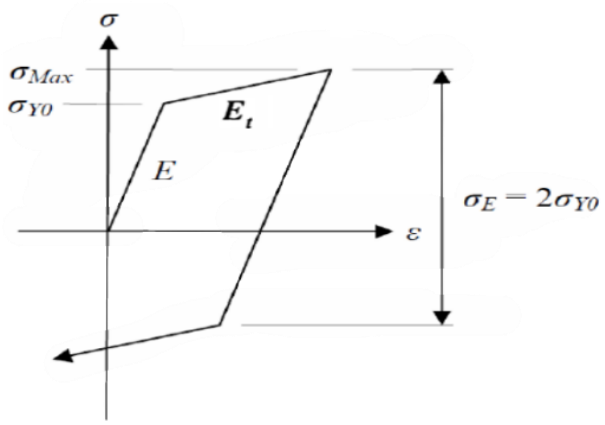

Figure 3.11: Bilinear kinematic hardening model [58].

3.10.2 Elastic Perfectly Plastic Model

A completely plastic model is the most straightforward way to represent the material's behavior. Figure (3-12) depicts this model's behavior. According to this concept, the yield point value in relation to plastic strain does not vary. This model's conclusions will not be significantly affected by the idealization of the plastic behavior of materials with low stress-hardness. In the elastic-perfectly plastic model, this is how the stress-stress connection is depicted. [58]

$$\varepsilon = \frac{\sigma}{E} \qquad (\sigma < \sigma_0) \tag{3.21}$$

$$\varepsilon = \frac{\sigma}{E} + \varepsilon^p \qquad (\sigma > \sigma_0) \tag{3.22}$$

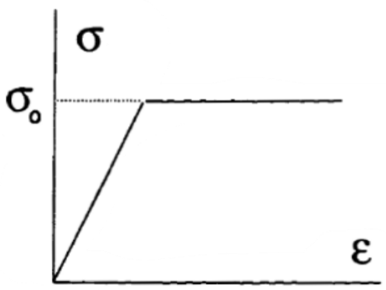

Figure 3.12: Elastic-perfectly plastic model [61]

3.10.3 Elastic-Linear Plastic Model

Elastic-linear plastic is a more realistic model than elastic-perfect plastic. In this model, the stress-strain curve is represented by two lines. Although the shift from elastic to plastic in the actual stress curve is often gentle, the change is abrupt in this model. With the material elastic module, the idealized graph's initial linear section has the same pitch. The second area describing the desired hardening behavior has a slope equal to the tangent module E_t. The stress-strain relationship for the elastic-linear plastic model may be represented as follows:

$$\varepsilon = \frac{\sigma}{E} \qquad (\sigma < \sigma_0) \qquad (3.23)$$

$$\varepsilon = \frac{\sigma}{E} + \frac{1}{E_t}(\sigma - \sigma_0) \qquad (\sigma > \sigma_0) \qquad (3.24)$$

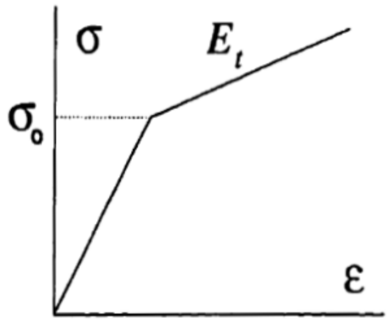

Figure 3.13: Elastic-linear plastic model

3.11 ENERGY SUMMERY

a. Kinetic energy is the power an object has because of its velocity. A force must be applied to a moving object in order that. cause it to speed up. Force makes us work. The object's speed will remain unchanged once work is done since energy has been transferred to it. This type of energy is called kinetic energy, and it is dependent on the recipient's newfound mass and speed. Transporting and transforming kinetic energy into other types of energy is possible. An example of such a situation would be a collision between a flying squirrel and an immobile chipmunk. It's possible that the chipmunk absorbed some of the squirrel's kinetic energy or that the energy was transformed into another form after the collision [62].

Following this line of reasoning, one must first determine the work done, **W,** by **a** force, **F**, before proceeding to compute kinetic energy. Let's say a force acting in a direction perpendicular to the surface moves a box of mass **M** a distance **D** along the surface. Given what has been discovered thus far:

$$W = F \cdot d$$

$$= m \cdot a \cdot d \qquad ...(3.25)$$

If we recall our kinematic equations of motion, we know that we can substitute the acceleration if we know the initial and final velocity (***v*i**, and ***vf)*** as well as the distance.

$$W = m \cdot d \cdot \frac{v_f^2 - v_i^2}{2d}$$

$$W = m \cdot \frac{v_f^2 - v_i^2}{2}$$

$$W = \frac{1}{2} \cdot m \cdot v_f^2 - \frac{1}{2} \cdot m \cdot v_i^2 \qquad ...(3.26)$$

Assume The initial velocity is zero and sub in eq (3.26) get:

Kinetic Energy: $K = \frac{1}{2} \cdot m \cdot v^2 \qquad ...(3.27)$

Alternatively, one can say that the change in kinetic energy is equal to the net work done on an object or system.

$$W_{net} = \Delta K$$

This result is known as the work-energy theorem and applies quite generally, even with forces that vary in direction and magnitude. It is important in the study of the conservation of energy and conservative forces.

b. Internal Energy: is the sum of all the particles' kinetic energy and chemical potential energy. When heat is added, particles accelerate and pick up kinetic energy [63].

c. Hourglass Energy: It's the effort put in by the opposing forces in order that offset the hourglass patterns. Non-physical, zero-energy, stress-free distortion modes called "hourglass modes" exist. Only under-integrated [Single Integration Point], solid shell, or thick shell components [with a single in-plane integration] lead to the emergence of hourglass modes. These can alter the accuracy of the solution by interfering with the genuine reaction of the structure, which in turn can provide inaccurate stress, strain, deflection, and contact predictions. When the energy of the hourglass is large in relation to the energy of the system itself, it's a positive sign that the hour glassing is severe and must be squashed further [64].

3.12 CONSERVATION OF MOMENTUM AND ENERGY IN COLLISIONS

For most collision types, forces are often unknown. Nonetheless, by utilizing the conservation principles of momentum and energy, we may derive a great deal of information about the motion after contact based on information gathered prior to the collision. Kinetic energy is preserved before and after collisions with extremely hard objects so that no heat or other kinds of energy are created. This type of collision is known as an "elastic collision." Consequently, in elastic collisions, the following is true for a system of particles [65]:

$$\left\{ \begin{array}{c} \text{Total kinetic energy before} = \text{Total kinetic energy after} \\ \sum \frac{1}{2} m v_{before}^2 = \sum \frac{1}{2} m v_{after}^2 \end{array} \right\} \left\{ \begin{array}{c} \text{Elastic} \\ \text{collision} \end{array} \right\} \quad \ldots (3.28)$$

Collisions in which kinetic energy is not conserved are referred to as inelastic. However, it is important to keep in mind that total energy is preserved even if kinetic energy is not. Thus:

$$\left\{ \begin{array}{c} \text{Total energy before} = \text{Total energy after} \\ \sum \frac{1}{2} m v_{before}^2 = \sum \frac{1}{2} m v_{after}^2 + \text{other forms of energy} \end{array} \right\} \left\{ \begin{array}{c} \text{Inelastic} \\ \text{collision} \end{array} \right\} \quad \ldots (3.29)$$

3.13 VEHICLE COLLISION DYNAMICS ANALYSIS

In automotive accidents, the collision event is a complex mechanical process. In terms of the car's mechanics, there is both the rigidity of the steel frame and the plastic deformation that happens when a certain force hits the car [66]. Due to the different quality, structure, speed, and the shape of the vehicles involved in the accident, the damage amount and how they move after the crash will be very different [67]. For the mechanics process involved in a car collision event, the fundamental mechanics theorem is used to simplify the model and do the relevant analysis and computation. The following assumptions are made to formulate the dynamic equation: The collision process is consistent with momentum conservation and does not take into consideration external forces. During the collision, the vehicle's mass distribution and shape do not change, and the frontal collision and collision impact are spread out evenly on the contact surface [68]. Based on the frontal collision hypothesis, it is possible to reduce the automobile collision process to a one-dimensional collision model. According to the rule of momentum conservation, the following can be deduced:

$m_1v_1 + m_1v_2 = m_1v_1' + m_1v_2'$

$$\Delta E = \frac{1}{2}(1 - e^{2})\frac{m_1 m_2}{m_1 + m_2}(v_1 - v_2)^2 \quad \text{... (3.30)}$$

The masses of the two colliding vehicles are m_1 and m_2, the speeds before the collision are v_1 and v_2, and the velocities after the collision are v_1' and v_2'. ΔE stands for the loss of mechanical energy after a collision, while **e** is the recovery coefficient between two vehicles.

3.14 AUTOMOBILE CRASHES HAVE THE FOLLOWING CHARACTERISTICS:

"Collision" is the process wherein two or more vehicles collide with one another or an object with sufficient force to transfer momentum, distort (usually plastically), and waste kinetic energy. The automobile shell rotates, moves, and deforms during a collision; plastic flow and material hardening occur; and contact friction at the border occurs. Though the collisions last only a few milliseconds each, they reveal a wealth of data about the collider. [69]. Strictly speaking, car crashes have the following properties:

a. The phenomena of transferring moving energy between vehicles.
b. Damage to both the body and the fixture, known as "mutual extrusion," decreases the energy of the motion.
c. It's a phenomenon in which certain parts are incompatible with one another, while others suffer harm from the interaction.
d. Not only is there an exchange of motion energy, but some motion energy is also turned into angular motion.
e. There is a lot of movement between the vehicles, the people, and the cargo.
f. Collisions happen in 0.1 to 0.2 seconds at low impact velocity, but at higher speeds, the time is fractions of a second.
g. A change in Collision Energy After a collision, the plastic deformation of the metal considerably increases the internal energy of the vehicle, transforming most of the kinetic energy into thermal energy. include transforming one kind of kinetic energy into another, like sound or heat. (Because of the internal energy gain, this is not a major concern in engineering.) [70].

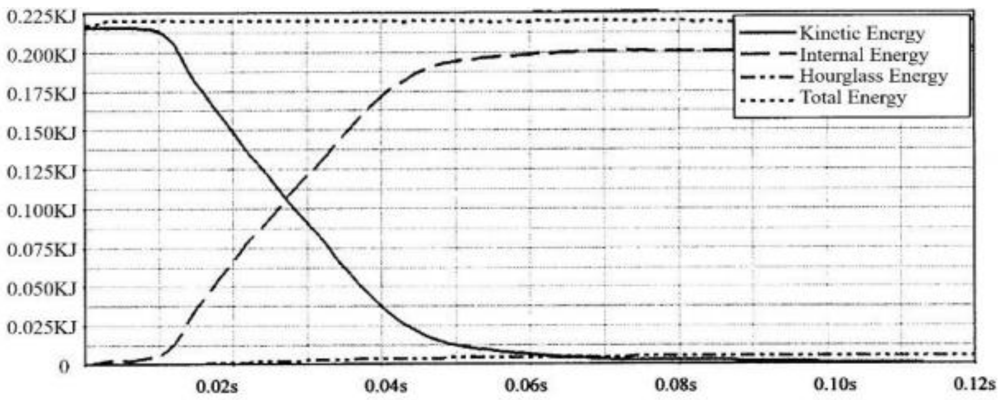

Figure 3.14: Vehicle collision energy curve [68]

Its kinetic energy is converted to thermal energy if it collides with a wall (or another object) and doesn't shatter. The vehicle's kinetic energy is converted into potential energy when it collides with an object, such as another vehicle. The foregoing is subject to the condition that the collision takes place on a level highway. If the impact takes place at an inclination, the potential energy gained from the contact will also be included in the energy conversion. Since objects are heated upon impact, collisions between them must result in energy loss (mechanical energy loss, which is kinetic energy loss in the absence of potential energy) according to the rule of energy conservation. The system's mechanical energy is preserved when conditions are ideal. Nothing in life is perfect. In practice, collisions are always elastically incomplete. During the collision, some of the mechanical energy will be converted to internal energy by inelastic deformation. The only way to bring the car to a halt is to transfer all of this energy into something else. If the brakes don't work properly, the energy is wasted as heat because of the friction. When a car is involved in a collision, the metal frames and bumpers absorb the impact by deforming and expanding. Vehicle frontal collision energy change curve shown in Figure (3-8).

3.15 MATCHING OF BUMPERS

3.15.1 Deflection and Energy Absorption Properties

Requirements for the elastic and energy-absorbing properties of bumpers, as well as their axial deflections. According to the notion of graded damage, it is assumed that such bumpers will protrude sufficiently in front of critical and non-vital automotive structures to reduce damage while also providing safety. These concerns do not require more discussion in this section [71].

3.15.2 Height Considerations

It is axiomatic that bumpers can only execute their safety and damage control roles if their height is uniform across all vehicle types. Even trucks and semi-trailers should, if feasible, be fitted with bumper devices at this specified height. Moreover, to maximize the safety of a person in a vehicle being struck on the side, the bumper of the other vehicle must strike a relatively stiff component of the vehicle being struck, which in this case is the frame. Consequently, the structure along the side of the vehicle should likewise be at bumper height. Obviously, bumpers should be needed to extend over the whole front and back dimensions of a vehicle, as well as around the four corners to the greatest extent possible. These standards are considerably at odds with current practice, where bumpers have become so mostly aesthetic rather than functional that several manufacturers of sport-type automobiles have eliminated their use altogether, particularly in the car's center sections.

3.15.3 Shape Considerations

In the horizontal plane, bumpers should be slightly convex in order to interface adequately with other bumpers over a variety of probable contact angles and to reduce the likelihood of pedestrians being needlessly injured. V-shaped or knife-edged protrusions, as well as the old-fashioned bumper guards that tend to fall off when lateral force is applied, serve no purpose. In a vertical cross-section, bumpers must contain adequate vertical dimension to ensure that they will still meet even if, in a rear-front 62 accident, the front end of the rear vehicle lowers due to the deployment of maximum brakes in an effort to avoid the collision. In addition to having adequate vertical dimensions, the vertical components of the bumpers should interact correctly, without a propensity to override or underride. Most modern bumpers feature a vertical cross-section that is circular at the top and then slopes rearward and downward, presumably mostly for aesthetic reasons. This bumper tends to ride over another car's bumper because of its current design, especially if its sloping sections may meet the round area of the bumper it collides with. The best protection may be provided if the vertical cross-section of bumpers is engineered to reduce the likelihood of override and underride, even under brake-dip circumstances. This aim may be achieved most effectively if the vertical cross-section is nearly flat at the tie interface. However, the potential benefits of substantial horizontal ridges to help in locking two impinging bumpers in a vertical direction should also be considered. In fact, such a modification would only be advantageous if the bumpers were insufficiently tall to perform their function without them.

3.15.4 Bumper Related Considerations

Offering safety-enhancing and damage-limiting bumper systems involve more than affixing a separate metal strip to the front and rear of a vehicle. If bumpers are constructed considerably higher to decrease brake dip, they must also be adequately supported to withstand the moment created by forces applied away from the vertical center. Their supporting and energy-absorbing structures, which are covered elsewhere in this study, must also be correctly built to channel impact forces back to the vehicle's frame. In addition, additional components of the vehicle must be built to adapt to such bumper systems. For instance, if a modern automobile were subjected to the impact pressures that well-built bumper systems might withstand without causing outward damage, it is entirely conceivable that other components, such as engine mounts, would fail as they are now intended. Therefore, these additional components must also be adequately reinforced to prevent harm.

3.16 BIONIC DESIGN INNOVATIONS INSPIRED BY NATURE

Honeycomb structures, whether they are natural or man-made, use the form of a honeycomb to facilitate the reduction of material consumed to reach the lowest possible weight and material cost. Though honeycomb constructions come in a wide variety of forms, they all have an arrangement of empty cells created by the juxtaposition of thin vertical walls. Standard cell shapes include columns and hexagons. A honeycomb-shaped material is light and strong in compression and shear when seen from an angle [72].

The in-plane crushing behavior of hexagonal honeycombs was studied by Hu et al., and the link between the three key parameters controlling the honeycomb's mechanical characteristics was determined. These include "the arrangement of the cells, the speed with which the cells are crushed, and the density of the honeycomb." [73]. the effect of the honeycomb's relative density is more pronounced at higher impact velocities, whereas at lower velocities the influence of the cell's geometric arrangement is more pronounced. This is based on the interpretation of the following diagram, which examines the "dependence of the normalized crushing strength on the cell-wall angle of honeycombs under x-directional crushing," in which the dashed curve of normalized density, also known as "the ratio of the honeycomb's density to the density of the regular hexagonal honeycomb," reaches its minimum value at an angle of 30 degrees before increasing with the angle of cell wall. This means that the regular geometric arrangement of honeycombs with 30-degree cell wall angles provides a good method to ensure stability in both axes in the construction of lightweight shell structures with hexagonal patterns under biaxial loading, as shown in figure (3-15) [73].

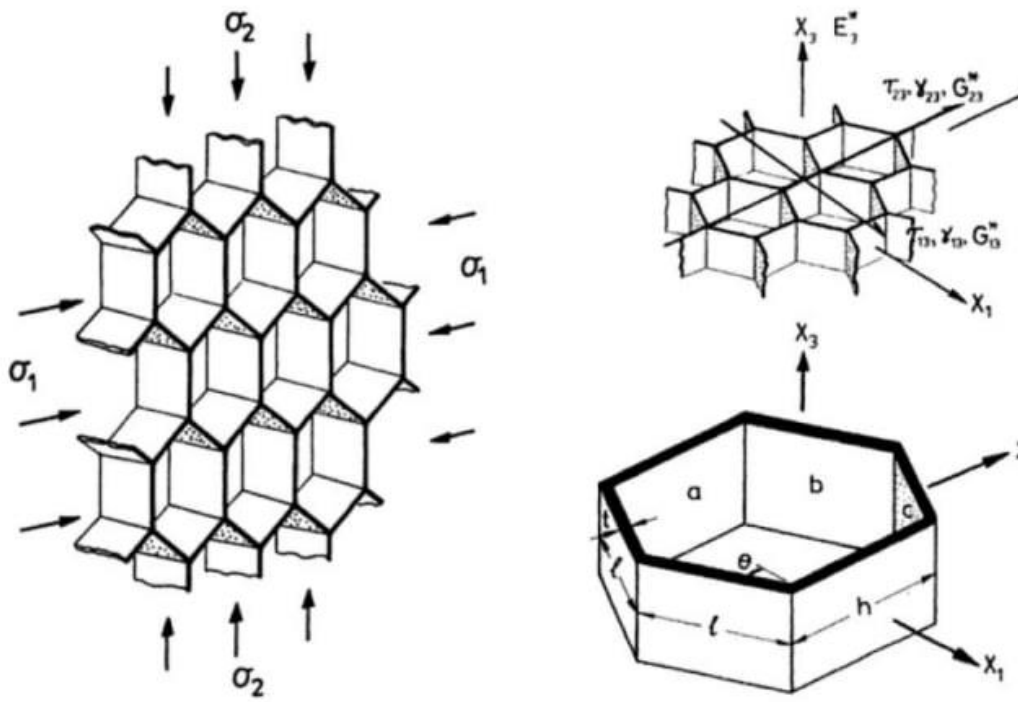

Figure 3.15: Biaxial loading in-plane and out-of-plane.

3.17 MATERIAL SELECTION

In the automotive industry, the process of reducing the weight of the car is an important element in this industry in order to reduce the rate of fuel consumption, as well as matters related to aerodynamics, as steel is the most important element in the process of manufacturing car parts and parts because of its high mechanical properties and low costs compared to other elements. The other, but with a higher weight.

Recently, the automotive industry has tended to use aluminum compounds with higher properties in the rate of energy absorption and less weight than compared to steel.

In this research, we will explain the metals that were selected in the simulation process and illustrate their mechanical and physical properties.

3.17.1 AISI 304 Stainless Steel

The austenitic chromium-nickel stainless steel AISI 304 (1.4301) is commonly employed. It possesses exceptional drawing qualities and outstanding formability, as well as strong corrosion resistance. 304 stainless steel is often used for sinks, kitchen tools like pots and pans, tubing, and a lot of other things.

Occasionally, Type 304 is sometimes referred to by its alternative moniker, 18/8, which comes from the fact that its typical chemical makeup consists of 18% chromium and 8% nickel. Silicon, Sulphur, nitrogen, phosphorus, carbon, and are among the other elements included in the alloy with nickel and manganese.

i. The Chemical Composition Of Aisi 304

(17.5-19.5%) chromium, (8-10.5%) nickel, (2%) manganese, (1%) silicon, (0.11%) nitrogen, (0.07%) carbon, (0.05%) phosphorus, and (0.03%) Sulphur are common constituents of AISI 304.

Table 3.1: Chemical composition of AISI 304 stainless steel [74].

ELEMENT	WEIGHT
IRON	**66.74 - 71.24 % (Balance)**
CHROMIUM	**17.5 - 19.5 %**
NICKEL	**8 -- 10.5 %**
MANGANESE	**2 %**
SILICON	**1 %**
NITROGEN	**0.11 %**
CARBON	**0.07 %**

PHOSPHOROUS	**0.05 %**
SULPHUR	**0.03%**

ii. Properties Of Aisi 304

Table 3.2: In the table, you can see some of the most common things about AISI 304.[74].

Density	7800 kg/m^3	**Elongation**	40%
Elastic modulus	193 GPa	**Coefficient of thermal expansion**	1.72E-5 1/K
Hardness, Brinell	215 HB	**Thermal conductivity**	16.2 W/(m·K)
Tensile strength	500-700 MPa	**Melting point**	1450°C
Yield strength	210 MPa	**Specific heat capacity**	500 J/(kg·K)
Poisson's Ratio	0.3	**Electrical resistivity**	0.73×10^{6} Ω·m

In addition to AISI 304 has great technical properties, like being resistant to corrosion and able to be machined, in addition to the ones listed above. the material properties listed above, AISI 304 has great technical properties like resistance to corrosion and the ability to be machined.

iii. Corrosion resistance

AISI 304 is very resistant to corrosion by most oxidizing acids. However, corrosion can occur in chloride-containing conditions. 304 stainless steel is less resistant to corrosion than 316 stainless steels.

iv. Machinability

AISI 304 has good machinability. Although AISI 304 does not transfer heat well, it needs to be cooled and oiled a lot, especially on the cutting edges.

3.17.2 Aluminum 7003 Series

Extruded aluminum bumper systems are found on more than half of all automobiles, ranging from the older and less expensive Chevrolet Cruz to the newly developed 2021 Ford Mustang Mach-E electric vehicle. The overall design of aluminum extruded bumper beams varies from vehicle to vehicle, but they often have many hollows within, a rectangular cross-section, and a curved curvature from side to side. Extruded bumper beams are utilized in automobiles with both internal combustion engine (ICE) and electric vehicle (EV) powertrains, as well as steel-intensive and aluminum-intensive body components. Aluminum alloys absorb more energy per unit of weight than steels with comparable yield strength. By increasing the gauge thickness, energy absorption may be boosted further. But since this would also make it heavier, it is better to pick a material with a higher yield strength.

For welded construction, AL 7003 is an extrusion alloy of choice. Features superior extrusion qualities than 7204 alloy. The strengthening of bumpers, sliders for motorcycle seats, frames for motorcycles, door impact beams, and wheels for motorcycles. AL-7003 is a super-strong extrusion alloy designed for use in very stressed structural applications. Scaffolding, mobile cranes, elevators, shipping containers, etc., are all common uses.

i. Chemical Composition Aluminum 7003

Table 3.3: Chemical composition ratio % of grade (AL-7003) [75].

Fe	Si	Mn	Cr	Ti	Cu	Zr	Mg	Zn
0.35	0.3	0.3	0.2	0.2	0.2	0.05-0.25	0.5 -1	- 6.5

ii. Properties Of The 7003 Series

Table 3.4: The table shows some of the material properties of the AL 7003 series [75]

Density	2800 kg/m^3	**Elongation**	10%
Elastic modulus	70 G P a	**Thermal expansion coefficient**	2.4*10-5 1/K
Hardness, Brinell	110 H B	**Thermal conductivity**	121 W/(m·K)
Tensile strength	330-350 M P a	**Melting point**	465 - 655 °C
Yield strength	255 M P a	**Specific heat capacity**	795 - 1050 J/(kg·K)
Poisson's Ratio	0.33	**Electrical resistivity**	5.6*10-8 Ω· m

iii. Corrosion Resistance

Due to its ability to easily form an oxide layer, 7003 series aluminum exhibits exceptional corrosion resistance. Further, aluminum oxide is an extremely sturdy substance. However, aluminum alloys change their behavior in high-salinity environments like seawater.

iv. Machinability

Aluminum can machine up to 3x to 4x faster than iron or steel.

3.18 AN INTRODUCTION TO THE METHOD OF FINITE ELEMENTS

The finite element method (FEM) is a numerical approach that may be used to solve a wide variety of problems in engineering and mathematical physics, including heat transfer, structural analysis, fluid flow, electromagnetic potential, mass transport and composite materials. Traditional methods of numerical integration, such as Euler's or Range- Kutta's, are used to solve transient problems, while the finite element method involves first transforming a physical problem explained by an ODE or a system of algebraic equations into a weak formulation, and then solving the resulting problem numerically. Values beyond the known range can be approximations at various points in the domain [58]. Finite elements are utilized to partition a very complicated issue into smaller, more manageable pieces, and their associated equations are then included into a larger, global system of equations that represents the entire problem/model. After deriving a global system of equations (variables methods from calculus of variations) from the problem's initial circumstances, the finite element method (FEM) uses them to estimate the solution by minimizing an error function.[76].

3.19” ELEMENTS TYPE IN FEM

The most common classifications are one-dimensional (1D), two-dimensional (2D), and three-dimensional (3D) elements (3D). It is important that all digital representations of physical structures be accurate representations. On the other hand, FEA isn't always the best choice for 3D solid components.

3.19.1 The Elements Of 1D

A one-dimensional element, or a node and a line between them, is the simplest possible element type. Even though they are all lines, one-dimensional components may have several degrees of freedom in their rotational and translational displacement functions [77]. Their primary use is in creating models of beams and trusses when the length substantially exceeds the width (or diameter) or thickness. They are also more successful when bending is the major cause of the issue, easier to model than 2D or 3D components, and provide a more accurate depiction of long members than solids. With the assumption that there are few significant changes in material properties throughout the cross section [78].

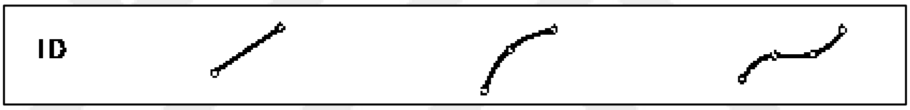

Figure 3.16: Represent 1D component with a variety of shapes.

3.19.2 D Elements

2D elements consist of three or four nodes and must be defined in the YZ plane. They are often referred to as shell elements or plates, and their fundamental forms are triangles or quadrilaterals. Examples of 2D components are the 3-node triangular element, 6-node triangular element [79]

When one dimension of a construction is thin relative to the others, they are used (thickness is small compared to other dimensions). While plates can withstand plane pressures, shell components can also withstand beam and torsion loads. It is used because, compared to 3D models, it takes less time to calculate and can describe thin shell structures.

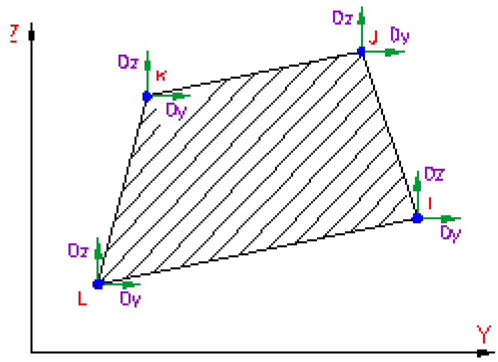

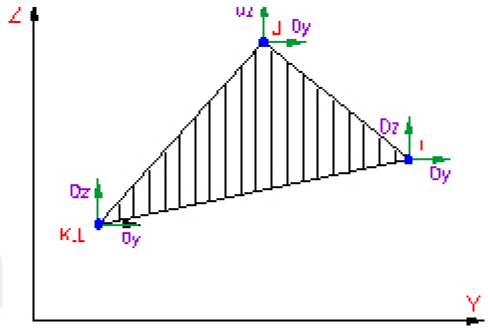

Figure 3.17: 2D elasticity elements (quadrilateral). **Figure 3.18:** 2D elasticity elements (triangular).

3.19.3 D Elements

Typically, 3D elements are utilized to mesh volumes. They are utilized in lieu of 1D or 2D elements when no dimension may be overlooked in relation to the others and the geometry is complicated. Three-dimensional (3D) finite elements provide greater diversity. There are three conventional geometries: the tetrahedron, the wedge, and the hexahedron (or "brick"). Additionally, there are two nonstandard geometries: the pyramid and the wrick, which have five and seven corners, respectively. Some examples of 3D elements are the 4-node tetrahedral element, the 10-node tetrahedral element, and the 8-node isoperimetric element. The most significant advantage of using three-dimensional parts is the ability to calculate deformations in all directions. Because of their very fine mesh, solid elements are the best at calculating stress, but they require more processing power and simulation time than 1D or 2D elements [80]

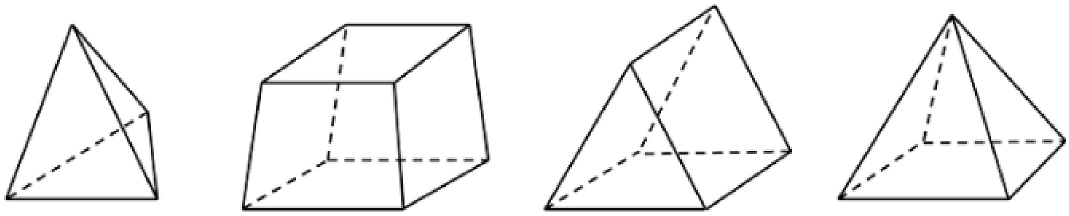

Figure 3.19: Shapes differed among 3D objects.

3.20 MODAL ANALYSIS FORMULA

The goal of modal analysis is to investigate the natural vibrational properties of a structure, such as [81]:

a. Frequency components found in nature

b. Modes of Normalcy (shapes)

Let f(t) = 0 and C = 0 (ignore damping) and obtain:

$M\ddot{u} + Ku = 0$ … (3.31)

Let's pretend that motion changes in a way that's harmonic with time:

$u(t) = \bar{u}\, sin(\omega t)$

$\dot{u}(t) = \omega\bar{u}\, cos(\omega t)$

$\ddot{u}(t) = -\omega^2\, \bar{u}\, sin(\omega t)$

where u is the nodal displacement amplitude vector. Substituting these into Equation (3.32) yields:

$[K - \omega^2 M] = 0$ … (3.33)

This is a generalized eigenvalue problem (EVP). The trivial solution is $\bar{u} = 0$ for any values of **ω** (not interesting). Nontrivial solutions $\bar{u} \neq 0$ exist only if:

$[K - {\omega^2}_i\, M]\bar{u}_i = 0$ … (3.32)

This is an nth-order polynomial of ω2 from which n solutions (roots) or eigenvalues ωi (i = 1, 2, …, n) may be determined. These are the structural natural frequencies (or characteristic frequencies). The frequency with the lowest nonzero eigenvalue, ω1, is known as the fundamental frequency. Equation (3.31) yields one solution or eigen vector for each ωi.:

$[K - \omega^2{}_i\, M]\bar{u}_i = 0$ … (3.32)

$\bar{u}_i$ (i = 1, 2, …, n) are the normal modes (or natural modes, mode shapes, and so on).

Properties of the Normal Modes:

Normal modes satisfy the following properties:

$$\bar{u}_i{}^T K \bar{u}_j = 0, \quad \bar{u}_i{}^T M \bar{u}_j = 0, for\ i \neq j$$

if **ω i ≠ ω j.** That is, modes are orthogonal (thus independent) to each other with respect to K and M matrices. Normal modes are usually normalized [81]:

$$\bar{u}_i{}^T M \bar{u}_i = 1, \quad \bar{u}_i{}^T K \bar{u}_I = \omega^2{}_i$$

Note:

a. In normal mode analysis, the magnitudes of displacements (modes) or stresses have no physical significance.

b. Normal mode analysis does not require any structural support.

c. ωi = 0 indicates that there are rigid-body movements of the entire structure or a portion of it. This may be used to validate the FEA model (See whether the FEA models have any loose or moving parts).

d. In FEA calculations, the lower the mode, the more precise it will be. This is because fewer elements/wavelengths are required for the lower modes, which have smaller spatial changes.

3.20.1 Modal Analysis For Example, Takes A Bumper System

Figure (3-20) depicts a car's front bumper and its supporting brackets. The model is used to investigate the bumper's dynamic responses. This study utilized shell components to determine the natural frequencies and vibration modes. Figure (3-21) illustrates the first mode of the bumper when limited at the bracket positions [81].

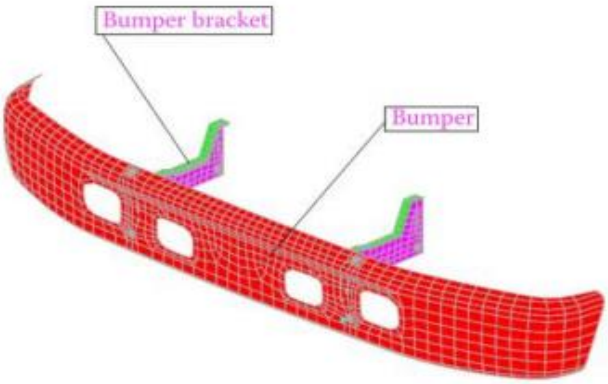

Figure 3.20: FEA model of a supporting brackets and front bumper.

Figure 3.21: The first vibration mode of the bumper.

3.21 THE STATIC FORCE-DEFORMATION TEST

The static force-deformation test was done by using Electronic Universal Testing Machine WDW-200E, as display in the shape (3-22). This test was executed at the University of Technology/Production engineering and metallurgy Department. The specimen was used full-scale size of the bumper beam as figure (3-23) illustrated.

Figure 3.22: Electronic Universal Testing Machine WDW-200E.

The sample was fixed from its ends of the absorber beam by bolts where the lower jaw is stationary while the upper jaw of the device moves down at a constant rate of (200 mm/min). A static force was applied to the sample gradually until the beam failed with the offsets (100 mm). The force-deformation curve was plotted directly on the test metric device's x-y recorder.

Brackets were utilized to secure the bumper to a stable foundation, allowing the static force-deformation characteristics of the bumpers to be evaluated. A rigid flat plate, like a hard wall in shape and measuring approximately in width, was used to crush the middle of the test bumper (20 cm).

Figure 3.23: A Full-Scale Size of the Bumper Beam Specimen.

4. NUMERICAL AND EXPERIMENTAL RESULT

4.1 THE NUMERICAL ANALYSIS

Many different branches of engineering and science are finding uses for finite element analysis (FEA). Making use of the proliferation of powerful, cheap, and easily accessible digital computers.

The approach is regarded as one of the most successful numerical methods due to its capabilities, which include complicated geometrical boundaries and nonlinear material characteristics. With the help of the ANSYS Workbench 22.R1 software, FEA is used as a numerical method to show how impact loads affect a structural feature so that the behavior of total deformation due to natural frequency can be evaluated.
The general analysis with ANSYS consists of three separate steps, including:

a. Developing model geometry
b. Apply the load-limiting criteria and arrive at the answer.
c. To investigate the outcomes.

4.2 BUILDING UP THE GEOMETRY

The ultimate objective of finite element research is to theoretically recreate the behavior of a real engineering system. In other words, the examination of a physical prototype must be based on an accurate mathematical model. The model consists of, in the broadest sense, all the nodes, components, material qualities, real constants / boundary conditions, and other characteristics needed to represent the physical system.

two different methods are used to create the model:

a. Modeling solid

b. straight generation.

With solid modeling, the model is automatically defined by its geometric bounds, but the size and desired shape of the components are controlled by set parameters. In contrast to the direct generation method, the position can be used to define the size, shape, and connection of each node and object before describing them in the model.

Solid modeling is typically more effective and flexible than direct generation and is generally the preferred method for generating models. As an alternative to creating solid models, the model can be created using a CAD system, and the export option makes the work between the CAD system and the ANSYS group so simple. ANSYS Workbench 22. R1 focuses mostly on Parasolid (x.t), Mechanical Desktop (.dwg), Solid Works (SLDPRT, SLDASM, etc.), and other similar programs.

The Parasolid (x.t) framework for exporting is therefore operational. Depending on how it grows (sat), the layout can be imported from the CAD framework into ANSYS Workbench 22.R1.

4.3. STRUCTURAL BUMPER DESIGN

4.3.1 Original Bumper Beam

The original bumper is blinding 3D geometry depending on an original model purchased from one of the agencies of the KIA company in Baghdad, the total mass for the model is 6.25 Kg, and the average thickness for the beam is 1.5 mm. figure (4-1) illustrates 3D using SOLIDWORKS 2016 software.

A lightweight bumper subsystem inspired by the Kia optima's transverse beam is now in the research phase. The actual frontal transverse beam was derived from a commercially available vehicle part and reverse engineered. All part's measurements were meticulously recorded so that inaccurate geometry representation wouldn't affect the bumper subsystem's real response to the impact. In order to generate the CAD model, we used SOLIDWORKS 2016 and the data we collected.

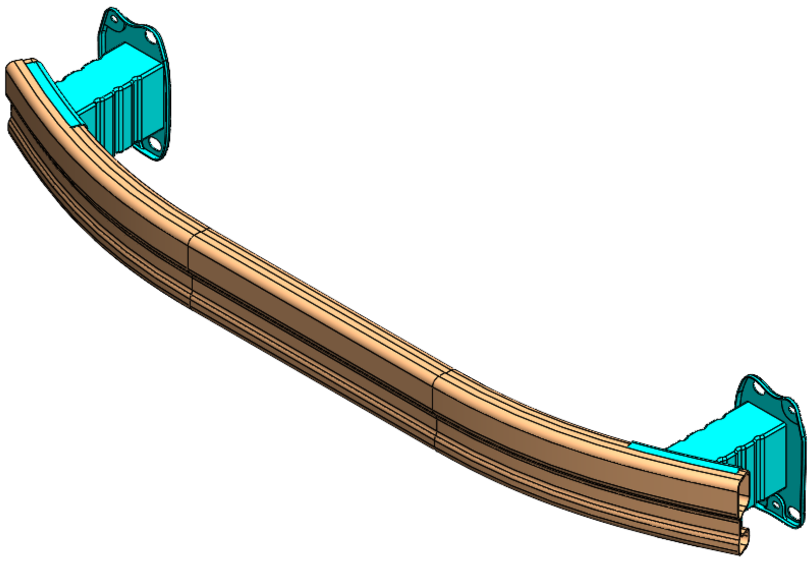

Figure 4.1: The Original 3D Bumper Beam Model from SOLIDWORKS.

4.3.2. Honeycomb Structure Bumper Beam

Bionic structure design depends on the dimensions of the original Kia bumper outside shape, but the inner cross-section is changed to a honeycomb hexagonal shape with the same the mass of the Honeycomb was calculated at approximately (6 kg) depending on the density of steel and geometric volume. The metal added to for hexagonal shape have less thickness approx. (1.25) mm; this is for the purpose of obtaining a weight similar to the original bumper which weighs approx. 6.25 Kg. Thickness when changing the metal from (Steel AISI 304) to (Aluminum), the mass of Bumper was calculated, approximately (3 Kg), meaning that the weight of Bumper was reduced to half the weight. The cross-section displays it in shape below (4-2).

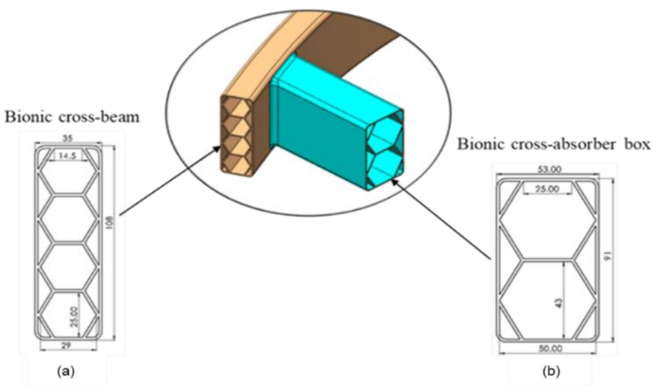

Figure 4.2: Dimensional details for the 3D Honeycomb Structural Bumper: (a) Bionic Cross-Beam and (b) Bionic Cross-Absorber Box.

4.4 THE MODELING OF FINITE ELEMENT

Research literature, actual working conditions, impact analysis, and bumper parameters, were all taken into account when developing the structural model of the bumper. The bumper structure and the shock endurance has been improved by repeating the bumper structure while considering different geometries, thicknesses, and workability. A dynamic behavior analysis using FEA software for each shock absorber structure has been performed iteratively to obtain an optimum shock absorber with better results. Furthermore, experimental confirmation of the improved natural frequencies was acquired from the fabricated fender using the FEA software.

Simulation steps of impacting the full-size rigid wall into a bumper beam:

a. Create a project for an Explicit Dynamics (ANSYS) Analysis System.
b. Choose a unit system and apply material characteristics.
c. Import the 3D geometry file format into Design Modeler (file extensions Parasolid x t).
d. Mesh the two pieces together and establish the rigid wall's starting velocity condition.
e. Set the analysis parameters, boundary conditions, and applied loads.
f. Start the solution (AUTODYN-STR) and check the outcomes.
g. Made linked interference between explicit dynamics and models as shown in figure (5) to calculate the mode shapes and total deformation under different natural frequencies.

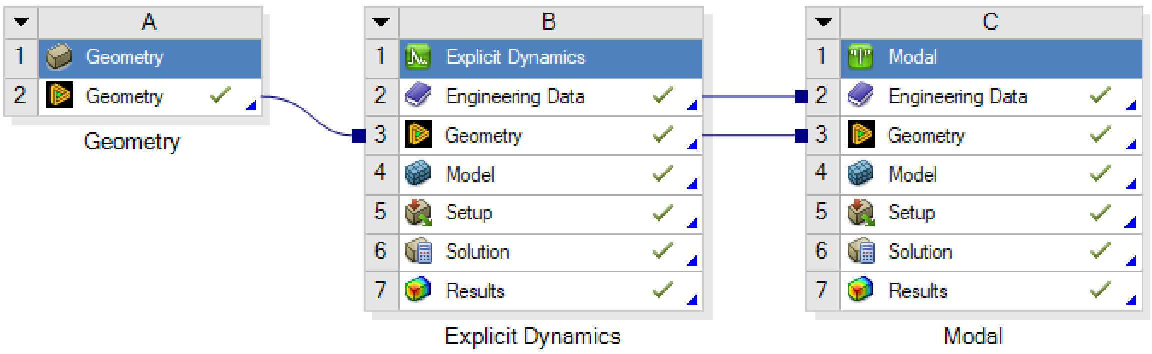

Figure 4.3: Linking Simulation Platform in ANSYS Workbench.

4.5 FINITE ELEMENT MODELING METHOD

In this study we used two workbench models:

a. Explicit dynamics approaches are better than implicit ones when it comes to structural problems that require complicated contact interactions in a short amount of time. So, the current investigation uses the commercial finite element software ANSYS/explicit dynamics to model how the bumper beam crash-box system worked during the car accident.

b. Naturally occurring frequencies, the provided system is calculated using the modal analysis component. Modal Analysis is the solution in ANSYS Workbench that calculates the resonance frequencies of any given shape under specified conditions. The form and restrictions of the geometry determine the resonance frequencies. The modal analysis also offers a depiction of the many modes of induced vibration. In other words, it depicts the many mode shapes that a structure exhibits during vibration. This form throughout different modes is known as a "mode shape," and each mode shape has its natural frequency. The modal analysis using ANSYS Solver allows the depiction of the mode shapes of both torsion and bending, as well as other mode shapes of any structure.

4.6 MATERIALS

After completing the export of the geometric shape file into the ANSYS program, the next step now comes to add the physical and mechanical properties that deform the elastic and plastic cases through the Engineer data portion for the two materials (steel AISI 304 & AL 7003) that represent the mechanical and physical properties.

4.7 SET SIZING CONTROL AND MESH MODEL

Meshing is perhaps the most critical aspect of any computer simulation since it can result in dramatic variations in outcomes. As illustrated explained in shape (4-4), the meshing procedure began with picking the element size using body sizing and then selecting the form of the element as a tetrahedron (Automatic meshing). The following steps were taken to make the mesh mechanism by selecting the mesh type (body sizing) and specifying mesh details as explicit and element size (3.5mm),

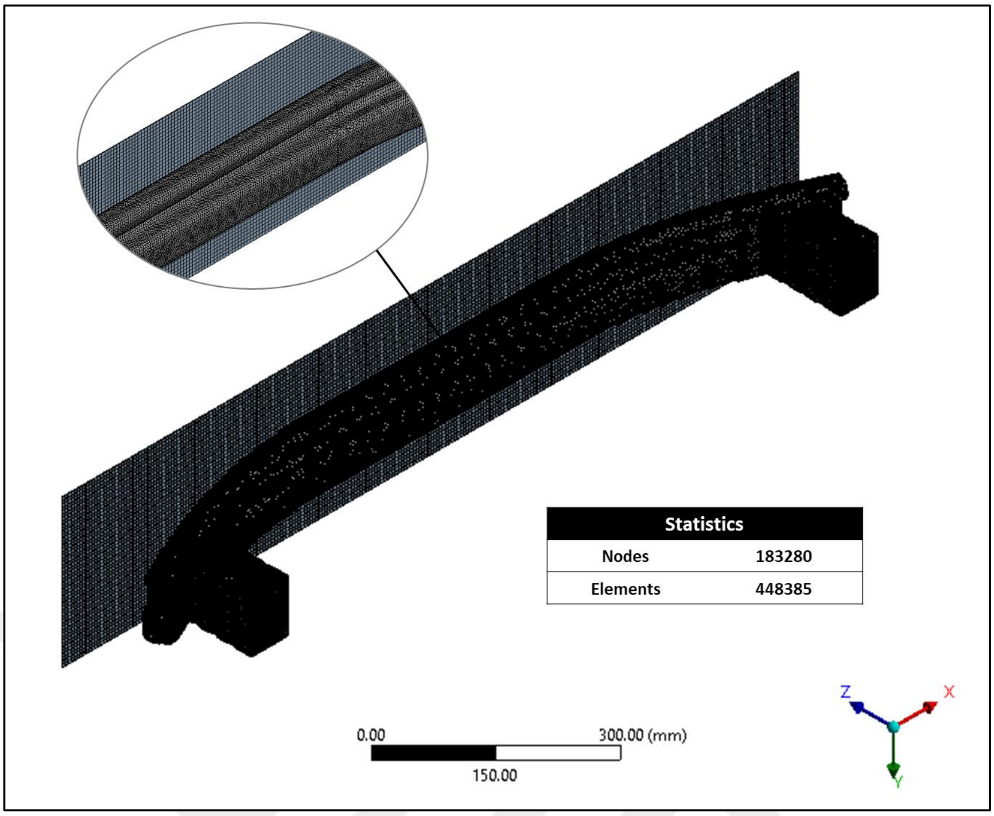

Figure 4.4: The Meshing of Bumper Specimens.

4.8 BOUNDARY CONDITION AND ANALYSIS TIME

In this research, simulations were used to analyze the effectiveness of bionic bumpers in absorbing energy. The bumper model was subjected to a frontal impact test, in which a complete stiff wall was employed as the point of impact. Three models were subjected to impact testing, whereby the height of a stiff wall mimicked that of an actual crash. Crash test circumstances were modeled as boundary conditions in the FE model, allowing kinetic energy conservation to be computed. Predicting the bumper beam's reaction in this way is the only way to do it. The full-size rigid wall has an initial velocity of (33.33 m/s) in the current FE model. As illustrated in figure (4-5), It was decided to define the initial velocity using z-axis components. Also, use the face selection filter to choose the rear face of the absorber box and set fixed support on the bumper beam's back face. In the detail view, choose the analysis setting from the tree and specify the end time (0.003 sec).

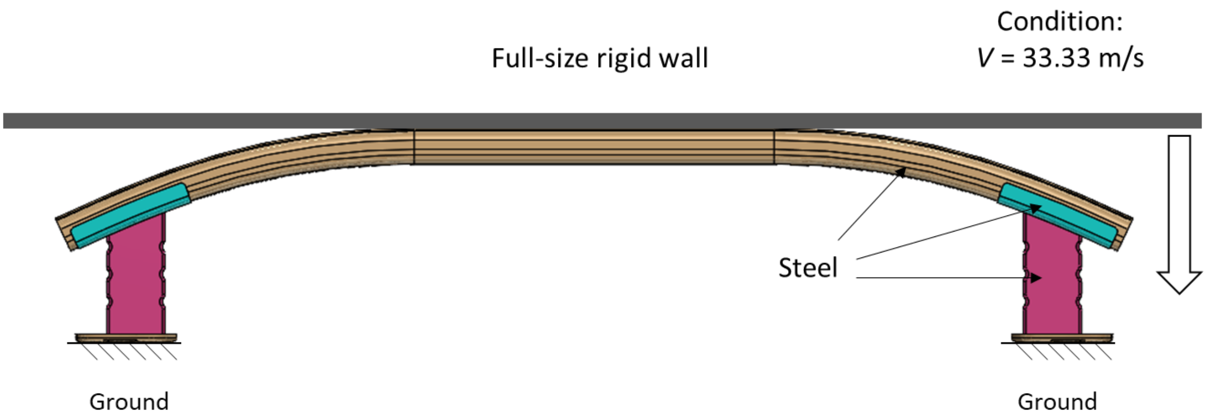

Figure 4.5: The Boundary Condition of the Impact Simulation.

Table 4.1: Show The Initial Boundary Conditions Setup For Explicit Dynamics.

Object Name	*Pre-Stress (None)*	*Velocity*
State	Fully Defined	
Definition		
Pre-Stress Environment	Non-Available	
Pressure Initialization	From Deformed State	
Input Type		Velocity
Define By		Components
Coordinate System		Global Coordinate System
X Component		0. m/s
Y Component		0. m/s
Z Component		-33.33 m/s

Table 4.2: Show The Analysis Settings For Explicit Dynamics.

Object Name	*Analysis Settings*
State	Fully Defined
Analysis Settings Preference	
Type	Program Controlled
Step Controls	
Number Of Steps	1
Current Step Number	1
End Time	3.e-003
Resume From Cycle	0
Maximum Number of Cycles	1e+07
Maximum Energy Error	0.1
Erosion Controls	
On Geometric Strain Limit	Yes
Geometric Strain Limit	1.5
On Material Failure	Yes
On Minimum Element Time Step	No
Retain Inertia of Eroded Material	Yes
Output Controls	
Step-aware Output Controls	No
Save Results on	Equally Spaced Points
Result Number of Points	20
Save Restart Files on	Equally Spaced Points
Restart Number of Points	5
Save Result Tracker Data on	Cycles
Tracker Cycles	1
Output Contact Forces	Off

Table 4.3: Show The Explicit Dynamic Loads & Fixed Support Faces.

Object Name	*Fixed Support*
State	Fully Defined
Scope	
Scoping Method	Geometry Selection
Geometry	2 Faces
Definition	
Type	Fixed Support
Suppressed	No

4.9 FULL-SIZE IMPACT ON EXPLICIT DYNAMICS SIMULATION RESULT

4.9.1 Convergence Analysis

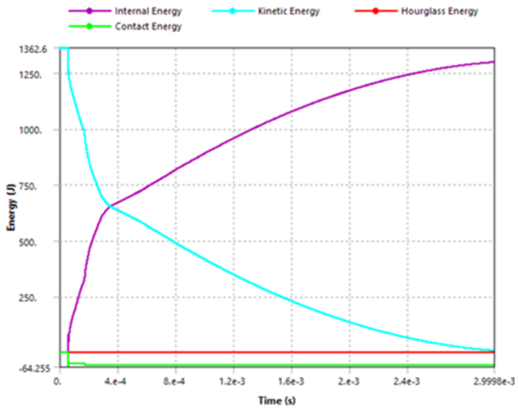

(a)

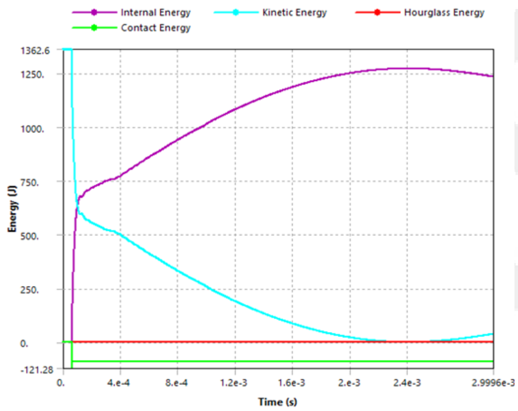

(b)

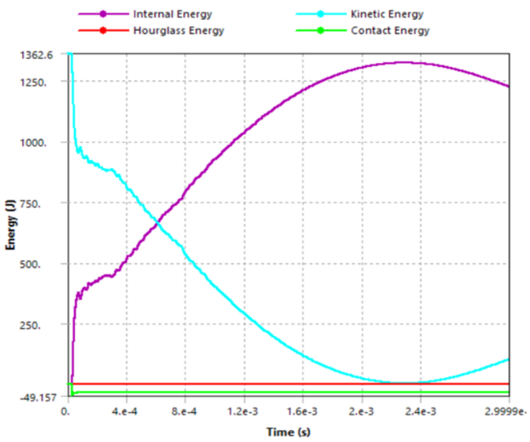

(c)

Figure 4.6: Energy Summary Graph for (a) Original Bumper and (b) Honeycomb Structural Bumper (steel AISI 304) (c) Honeycomb Structural Bumper (AL 7003).

4.9.2 Total Deformation Result:

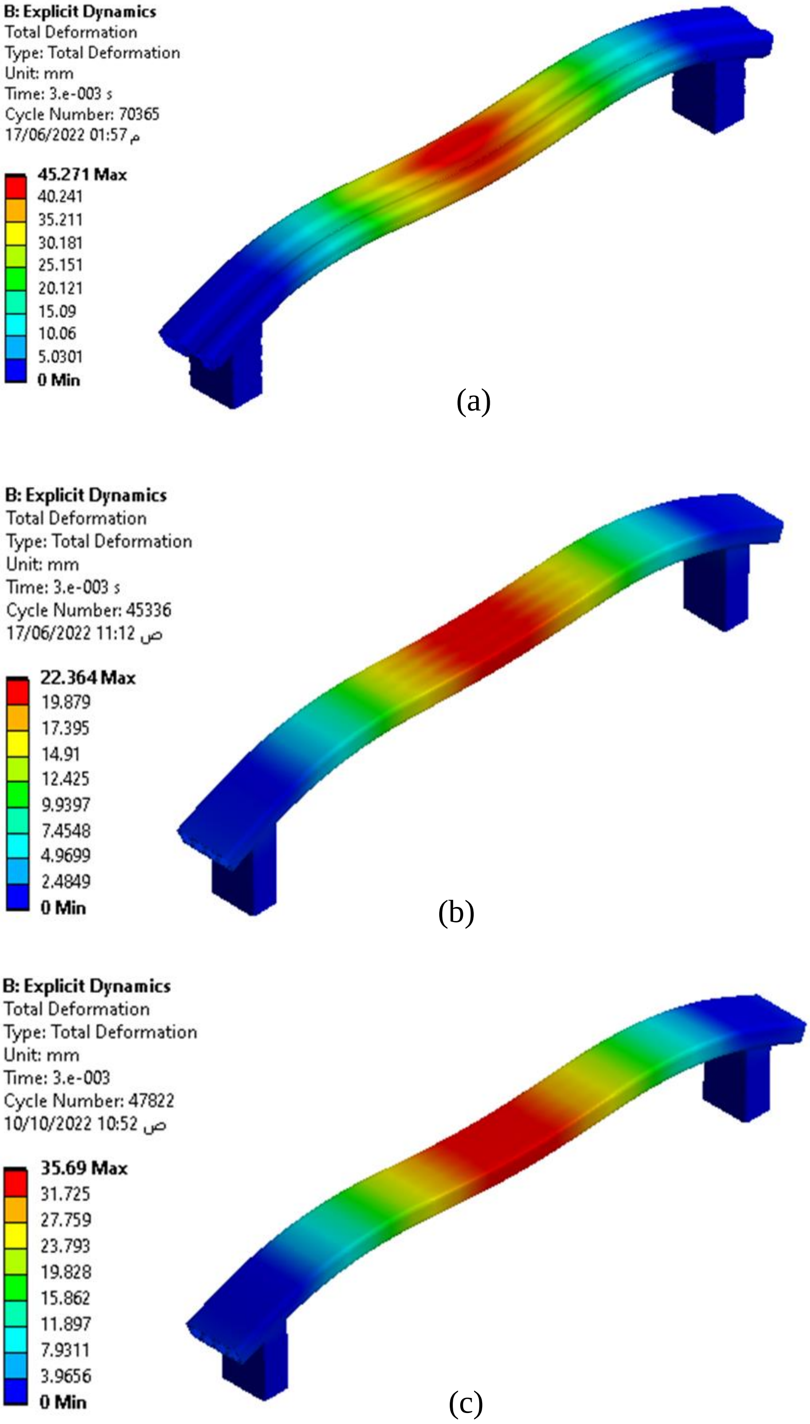

Figure 4.7: Total Deformation Contours at Time (0.003 sec) for: (a) Original bumper (b) Honeycomb Bumper (Steel AISI 304) (c) Honeycomb Bumper (AL 7003).

4.9.3 Equivalent (Von-Mises) Stress Result:

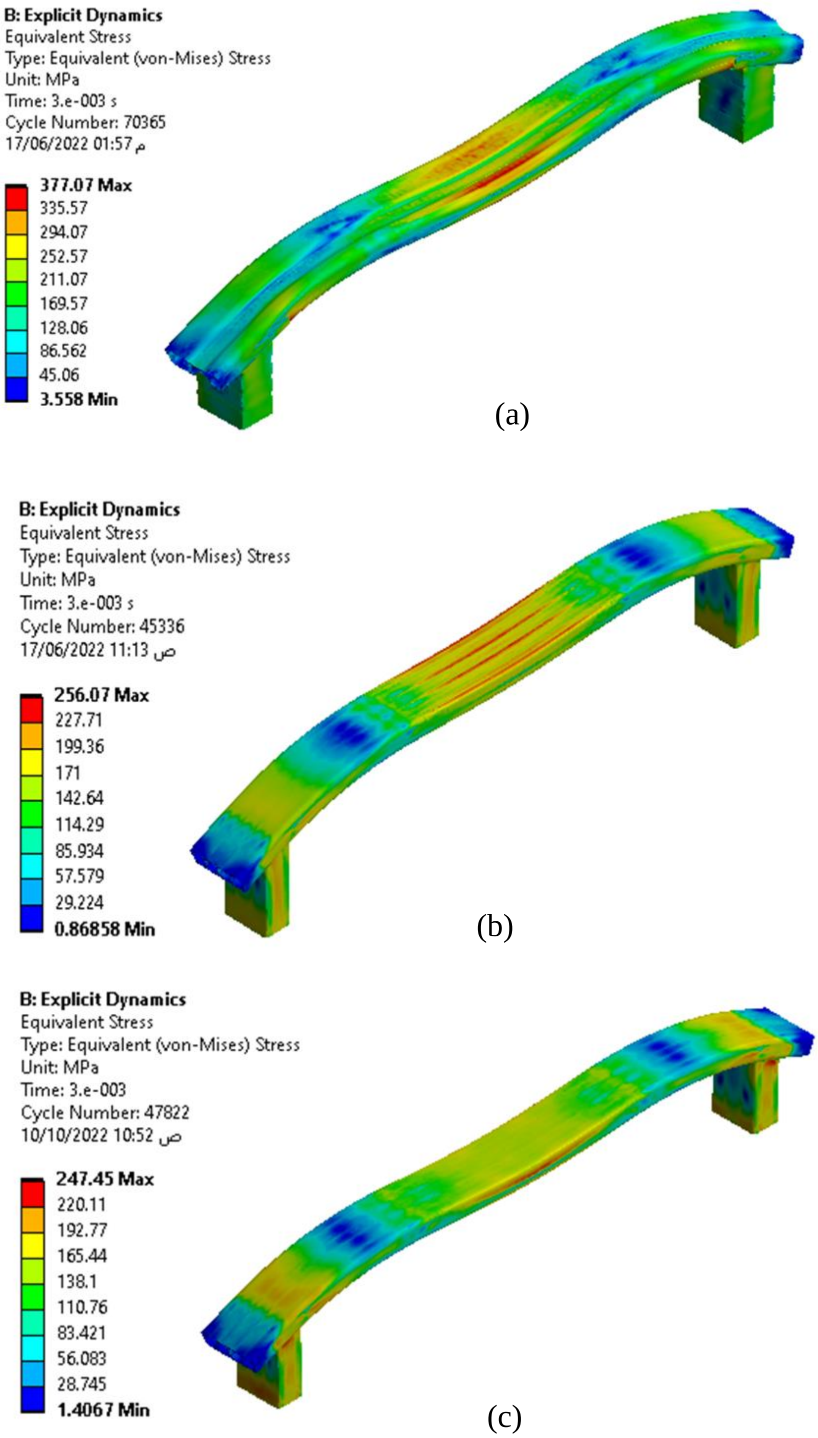

Figure 4.8: Equivalent (Von- Mises) Stress Contours at Time (0.003 sec) for: (a) Original bumper (b) Honeycomb Bumper (Steel AISI 304) (c) Honeycomb Bumper (AL 7003).

4.9.4 Equivalent Elastic Strain Result:

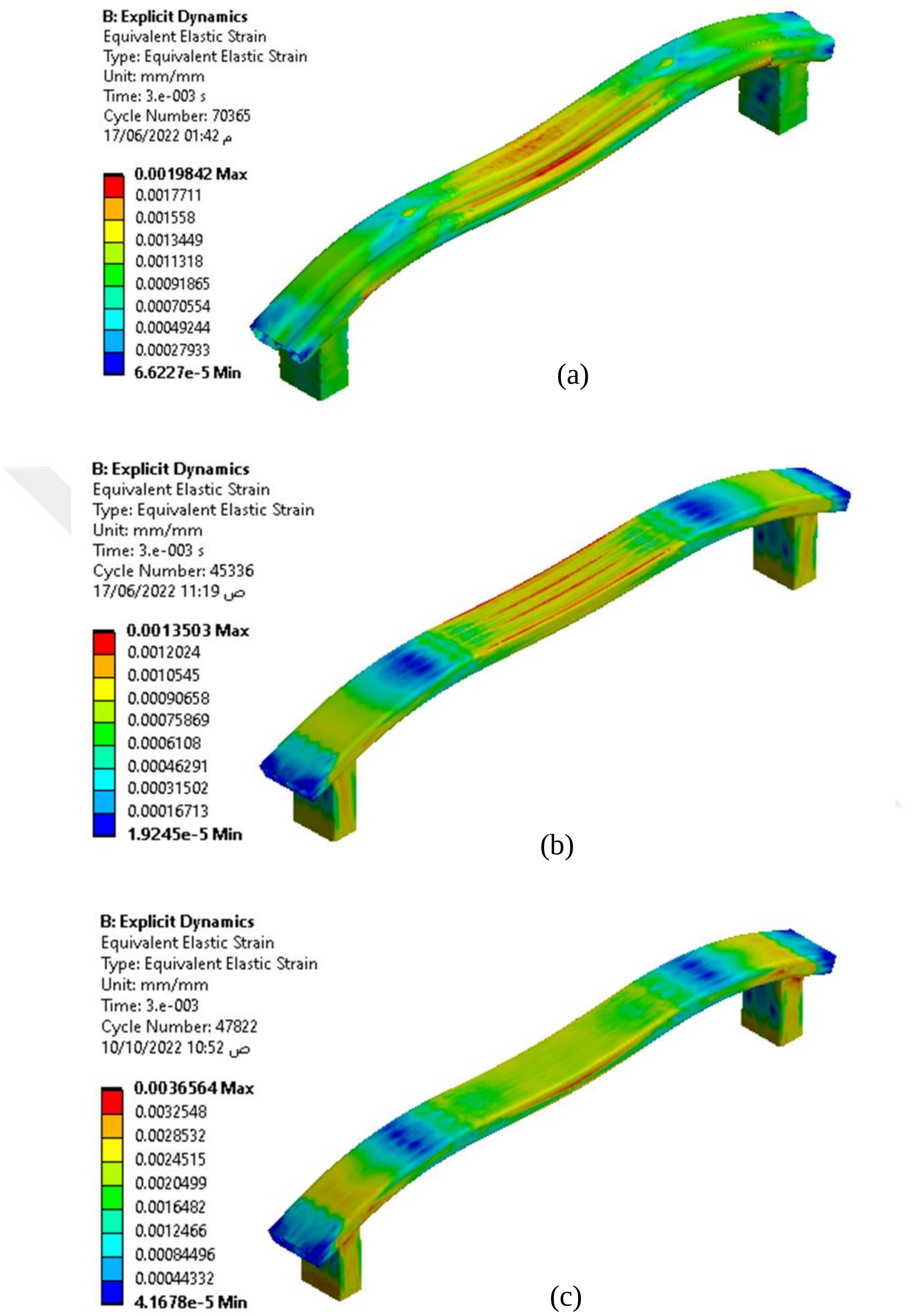

Figure 4.9: Equivalent Elastic Strain Contours at Time (0.003 sec) for: (a) Original bumper (b) Honeycomb Bumper (Steel AISI 304) (c) Honeycomb Bumper (AL 7003).

4.9.5 Equivalent Plastic Strain Result:

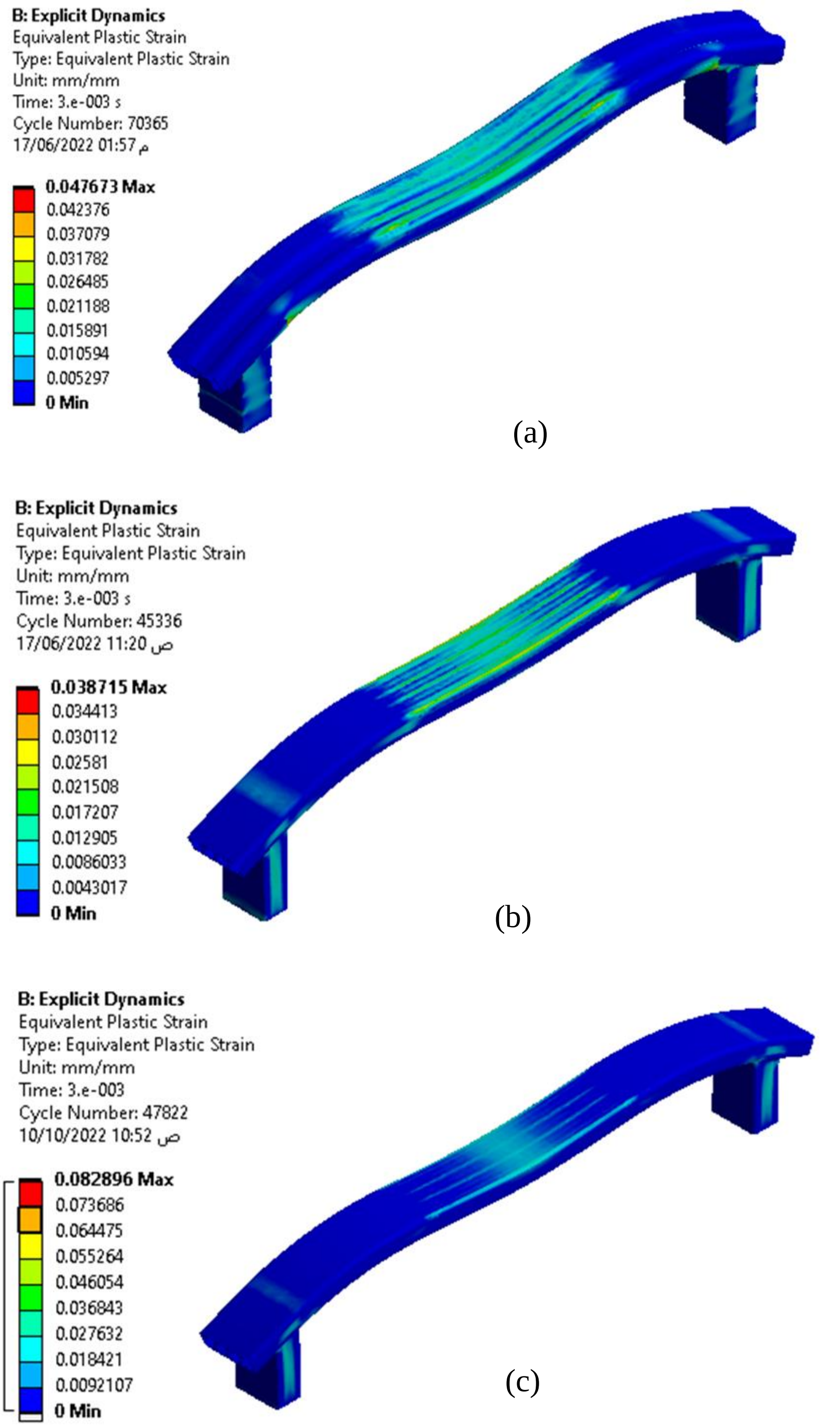

Figure 4.10: Equivalent Plastic Strain Contours at Time (0.003 sec) for: (a) Original bumper (b) Honeycomb Bumper (Steel AISI 304) (c) Honeycomb Bumper (AL 7003).

4.10. NATURAL FREQUENCY (MODEL SIMULATION) RESULT

4.10.1 Original Bumper:

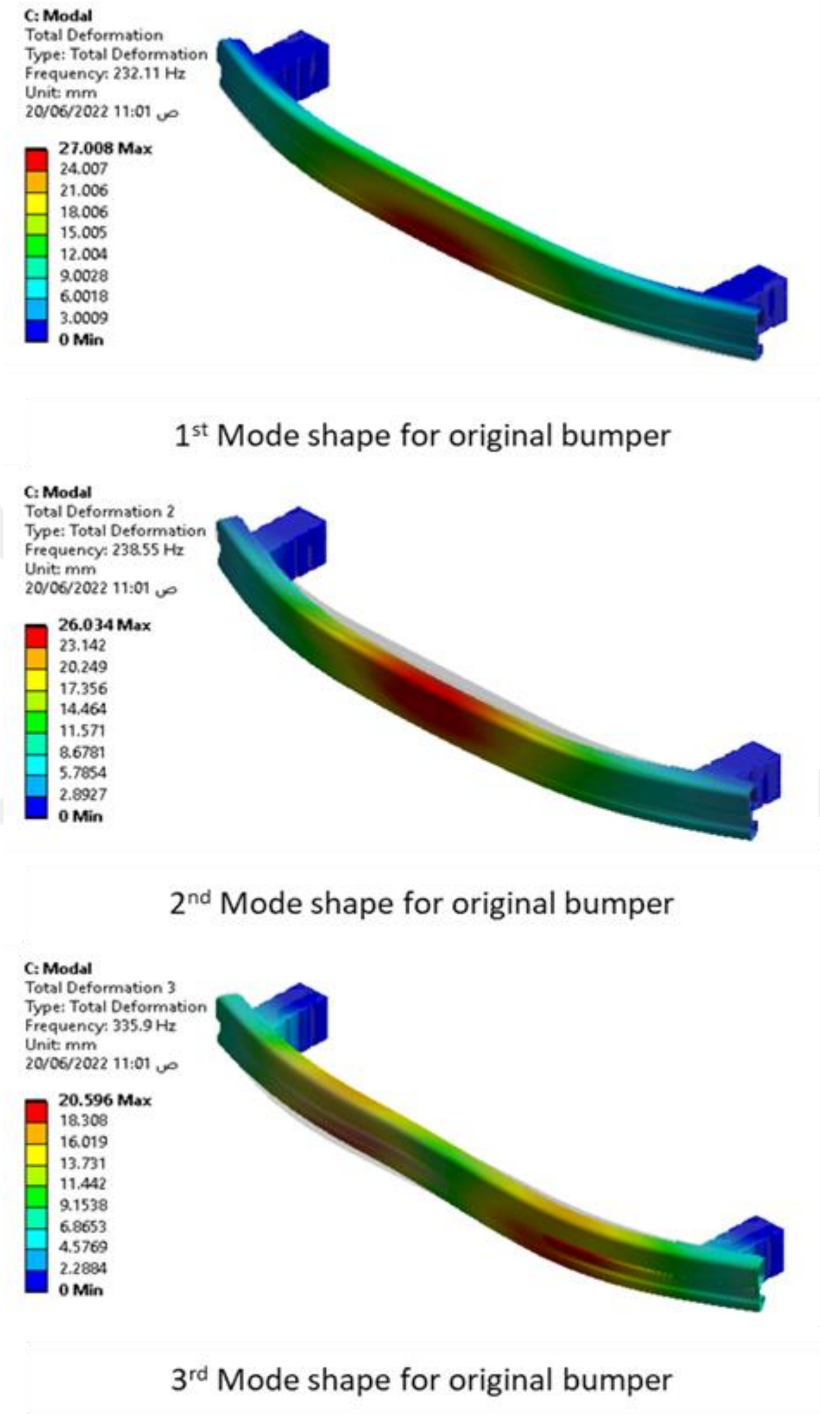

Figure 4.11: Total Deformation from Modal Analyses the First Three Mode Shapes of Original bumper Model Obtained through ANSYS.

4.10.2 Honeycomb Bumper (Steel AISI 304)

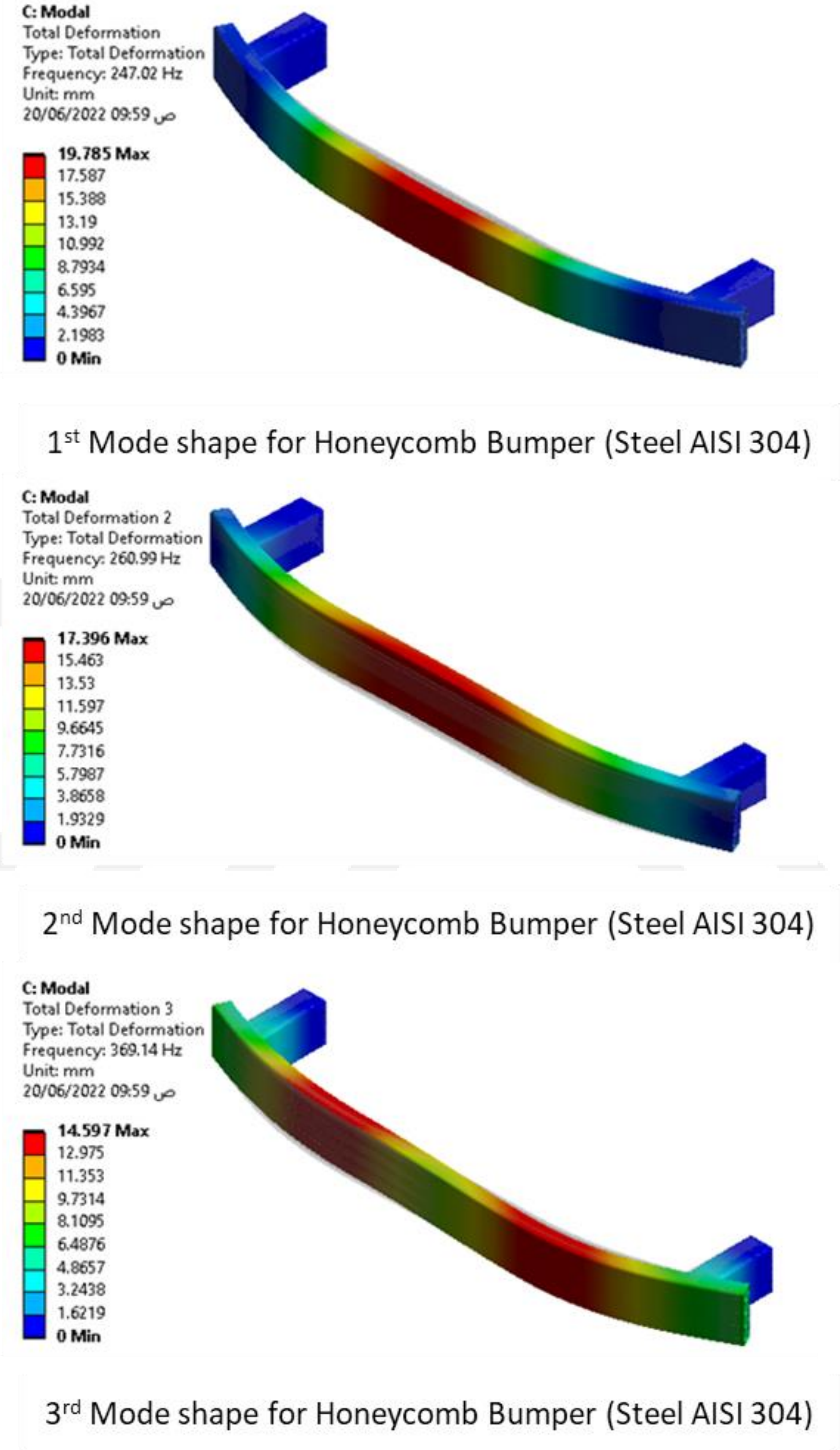

Figure 4.12: Total Deformation from Modal Analyses the First Three Mode Shapes of Honeycomb Bumper (Steel AISI 304) Model Obtained Through ANSYS.

4.10.3 Honeycomb Bumper (AL 7003)

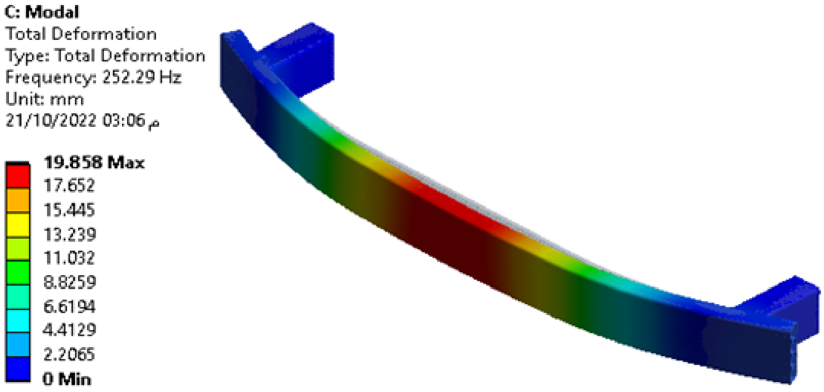

1st Mode shape for Honeycomb Bumper (AL 7003)

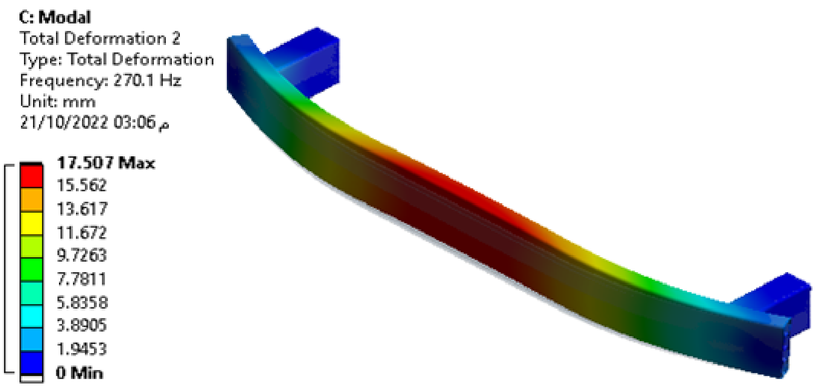

2nd Mode shape for Honeycomb Bumper (AL 7003)

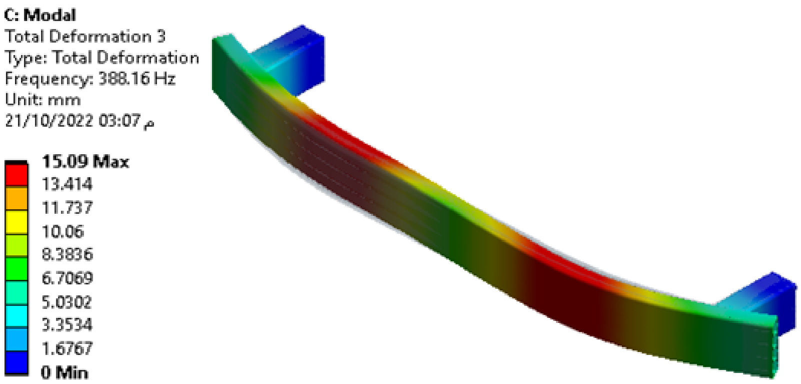

3rd Mode shape for Honeycomb Bumper (AL 7003)

Figure 4.13: Total Deformation from Modal Analyses the First Three Mode Shapes of Honeycomb Bumper (AL 7003) Model Obtained Through ANSYS.

4.11. EXPERIMENTAL RESULT:

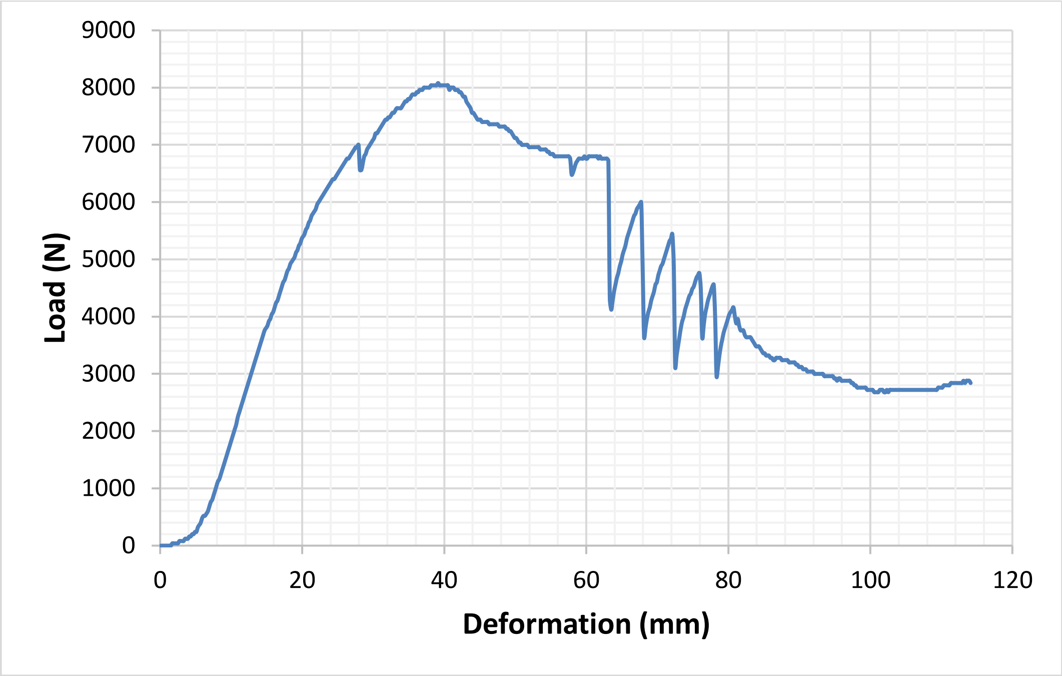

Figure 4.14: The relationship curve between (Load vs Deformation) Obtained through experimental Test.

Figure 4.15: The picture shows the shape of the original bumper of the KIA Optima 2019 after being deformed

5. THE DISCUSSION AND CONCLUSION

5.1. NUMERICAL SIMULATION DISCUSSION

5.1.1. Explicit Dynamics Discussion

a. Convergence Analysis: Because the finite element technique is a way of arriving at an approximation of the correct answer, the error that is produced should be limited to a bare minimum. The mesh-convergence analysis is one method for determining whether or not the data is accurate. It is important to define the range of mesh sizes across which reliable results may be obtained. In the convergence analysis, the quantity of potential energy stored in the bumper is used as the regulating variable. The data illustrated in figure (4-6) indicates a value of around 1.3 kilojoules of internal energy, yielding results that are precise enough for their intended application.

b. Impact Energies: After the impact, the amount of kinetic energy transferred from the wall to internal energy in the bumper is the amount of absorber energy. by designing the bionic bumper structure with collision capabilities in mind during a forward collision. When the energy charts of both bumpers (hexagonal shape and original shape) are compared, it is revealed that the bumper with an adjusted cross-section has more internal energy absorption capability.

Following the collision, an increase in internal energy absorbed of 15% was seen when the cross-sectional area was enhanced to honeycomb hexagonal (AISI 304), as well as an improvement in plastic energy of 18.2% compared to the original design. But when used (AL7003), it appears that the average internal energy (1323.5 J) is very close to that of the original bumper. Figure (5-1), (5-2) and (5-3), the Changing of Internal, kinetic and plastic During the Impact Period (0.003 sec) for three cases.

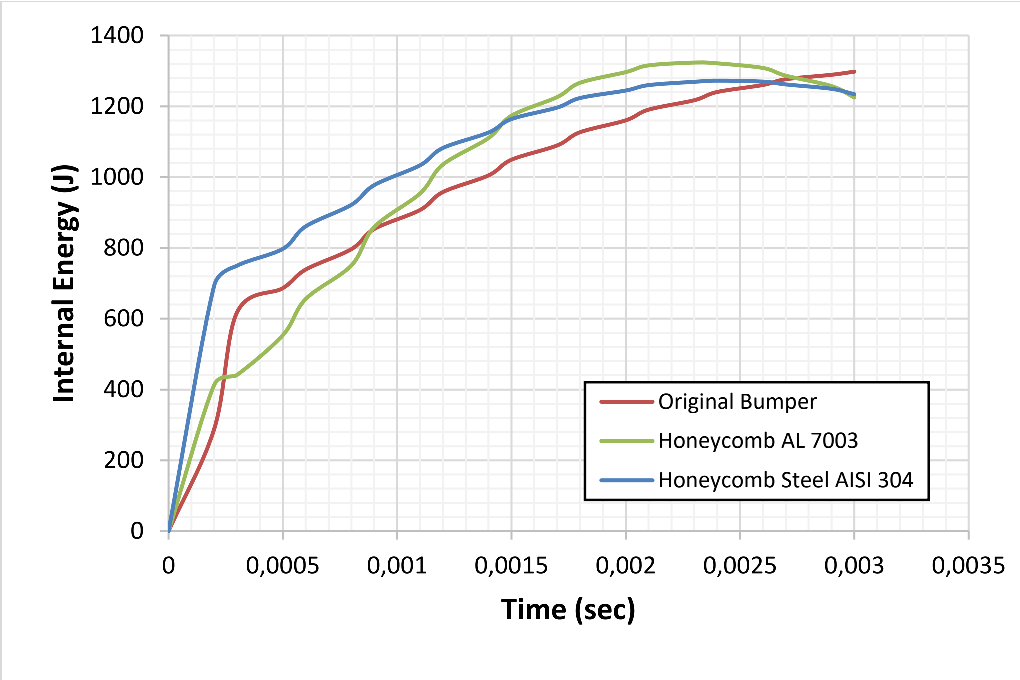

Figure 5.1: The Changing of Internal Energy During the Impact Period (0.003 sec) for three cases.

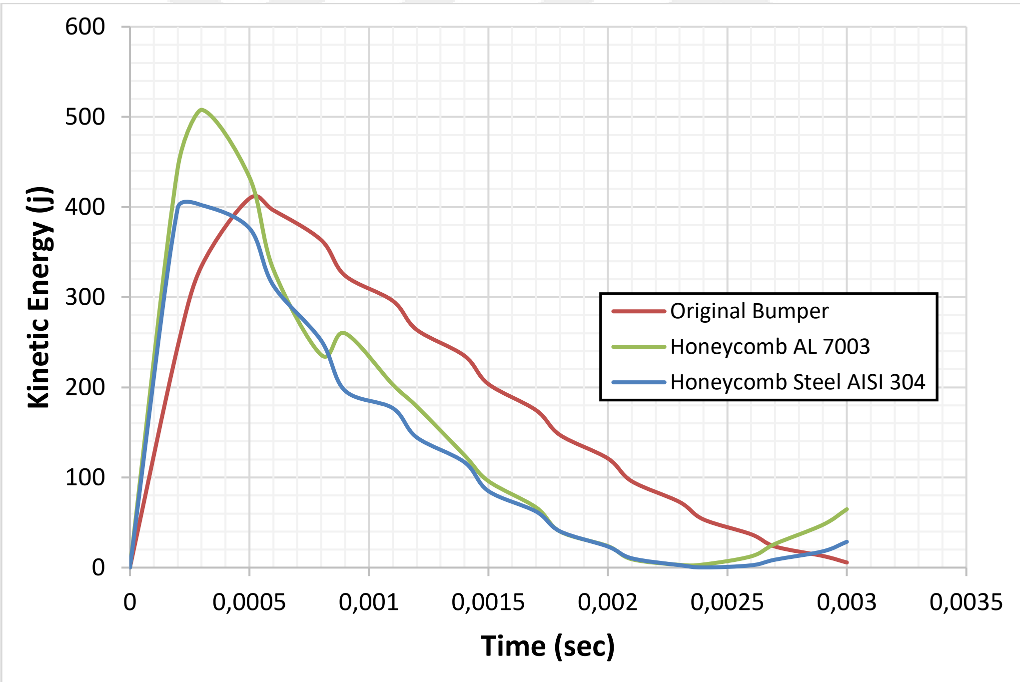

Figure 5.2: The Changing of Kinetic Energy During the Impact Period (0.003 sec) for three cases.

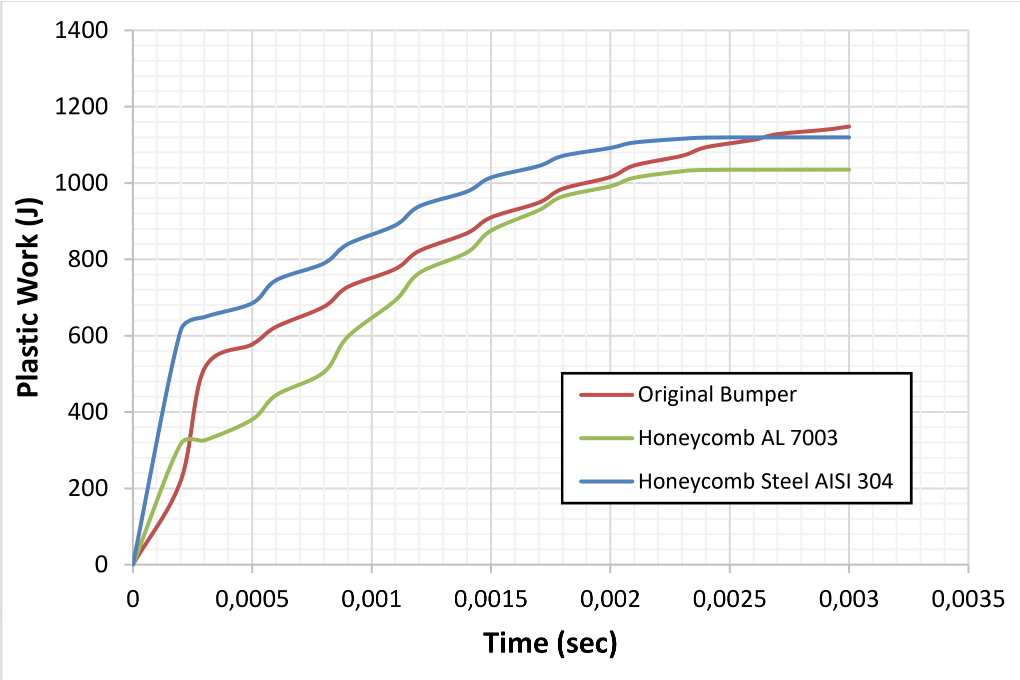

Figure 5.3: The Changing of Plastic work During the Impact Period (0.003 sec) for three cases.

c. Stress Distribution and Total Deformation: Figure (4-7) shows the deflections that occurred in the vehicle's front bumper beams. For the original bumper, the maximum total deformation attained after the impact duration is (45.27 mm). The Honeycomb hexagonal-shaped (Steel AISI 304) bumper caused reduced deformation of approximately (22.36 mm) with parentage of redaction is (47.18%), which happened in the vehicle's front bumper beam at the same boundary condition of collision. And for same geometrical (Honeycomb hexagonal) shape with using (AL 7003) the maximum total deformation will be higher than steel model but less than original bumper with parentage approximately (11.089 %). while reducing the weight of the bumper approx. 49.09 %. Figure (5-4) demonstrated the difference between the three models in terms of their resistance to deformation.

The stress distribution of the vehicle's original front bumper is shown in figure (4-8a). The highest equivalent stress obtained is (377.07 MPa), which is significantly beyond the yield strength of the material, indicating that the bumper has entered the plastic zone and has begun to deform plastically. The highest equivalent stress for a honeycomb hexagonal (Steel AISI 304) bumper is explained in the shape below (4-8b). The maximum stress concentration was found at the sharp edges, which are the areas of connection of the absorber part with the beam bracket. And for same geometrical (Honeycomb hexagonal) shape with using (AL 7003) the highest equivalent stress obtained is 247.45 MPa that value less than original bumper in percentage of the amount

(19.41%). But in this case, the beam would have crossed the yield zone and appeared to deform the plastic.

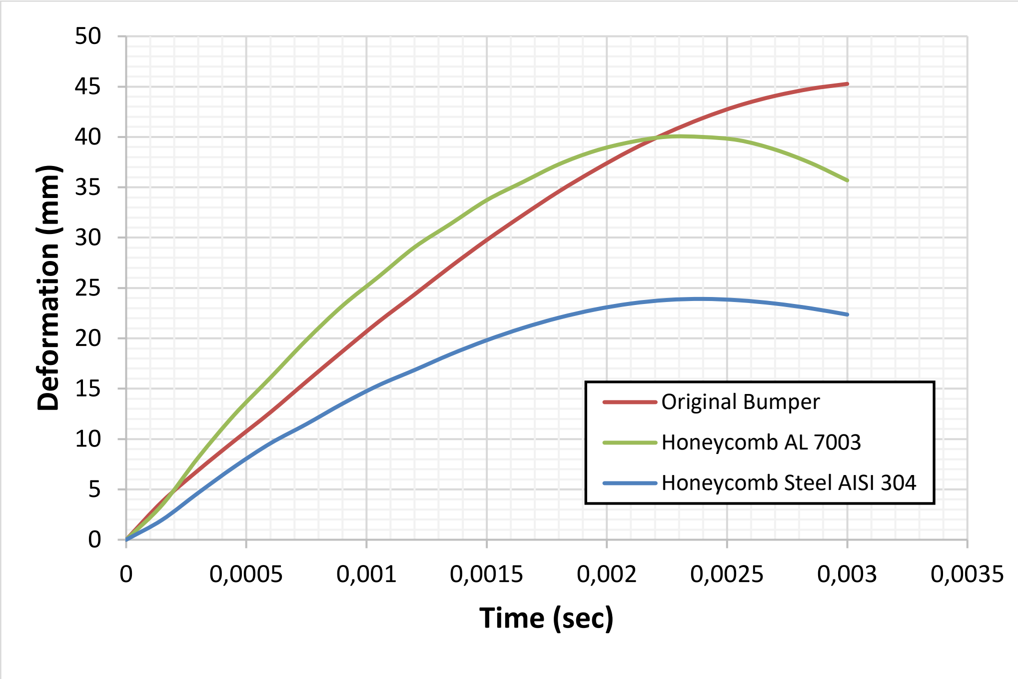

Figure 5.4: Relation Result Curve after Impact Period (0.003 sec) for Total Deformation.

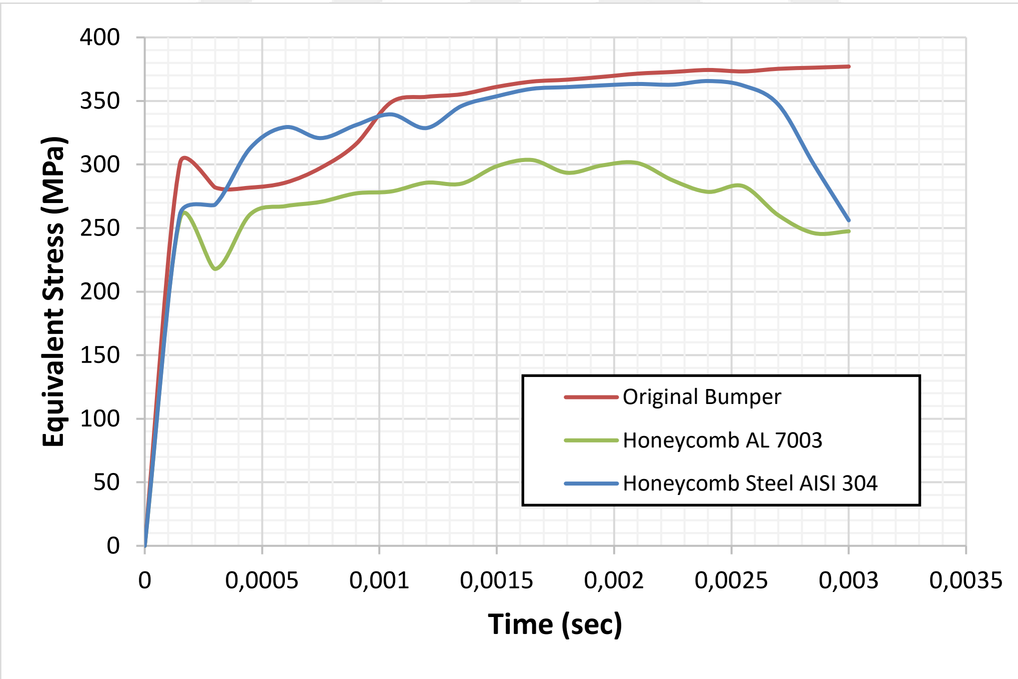

Figure 5.5: Relation Result Curve after Impact Period (0.003 sec) for Equivalent Stress.

d. Equivalent Elastic and Plastic Strain: they play an important factor in indirect the failure change in geometry shape which was changing during the impact force. The maximum equivalent elastic strain for the original bumper is (0.00198 mm/mm) Compared with the Honeycomb (Steel AISI 304) bumper (0.00135 mm/mm). Figure (5-6) illustrate the behavior of elastic deformation change. The plastic impact made permanent deformation can observe in figures (4-9) and (4-10). Also, the equivalent plastic strain for the original beam is reduced from (0.04767 mm/mm) to (0.03872 mm/mm) in the Honeycomb (Steel AISI 304) beam and it is increased when used Honeycomb (AL 7003) beam about (0.0829).

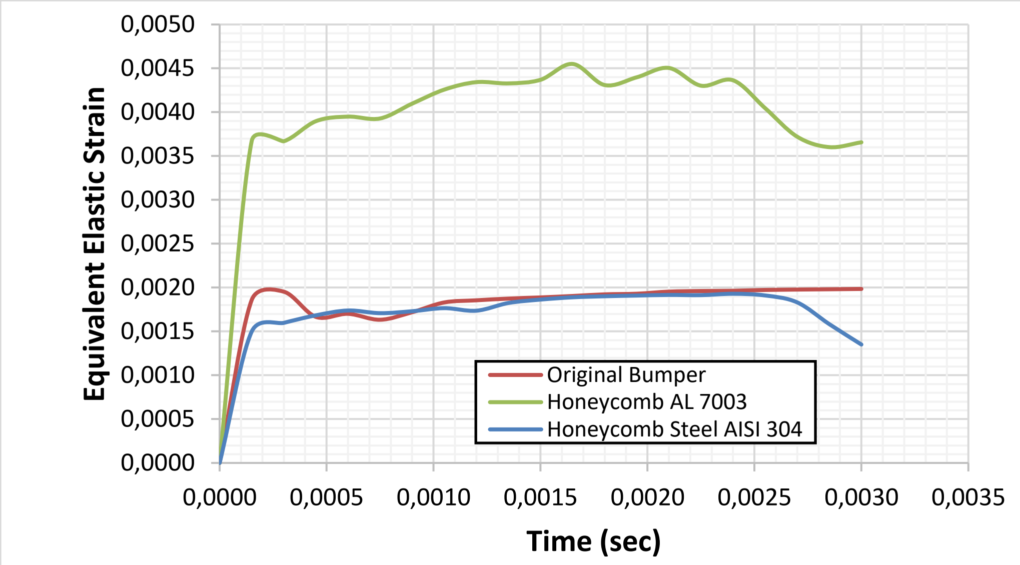

Figure 5.6: Relation Result Curve after Impact Period (0.003 sec) for Equivalent Elastic.

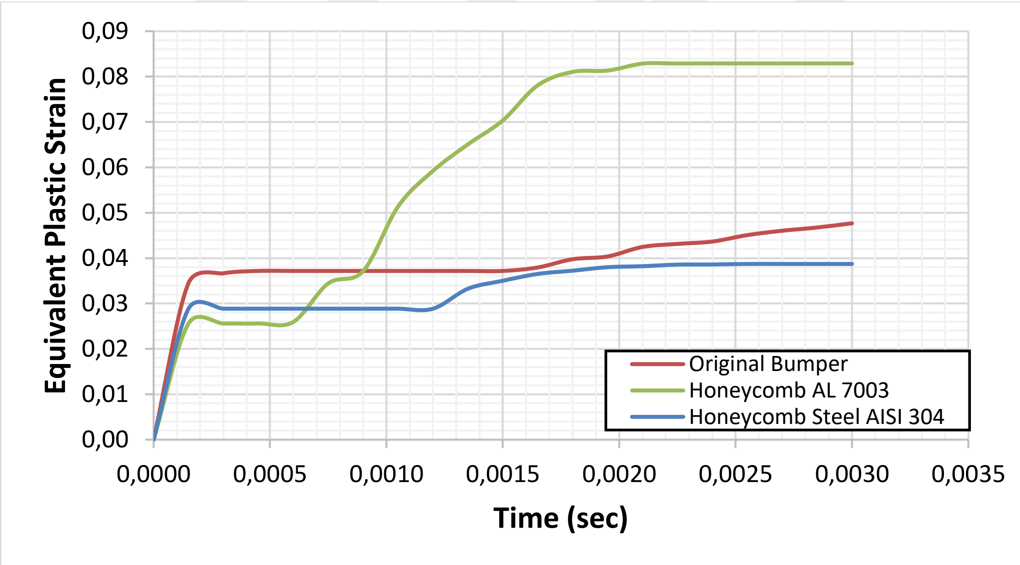

Figure 5.7: Relation Result Curve after Impact Period (0.003 sec) for Equivalent Plastic.

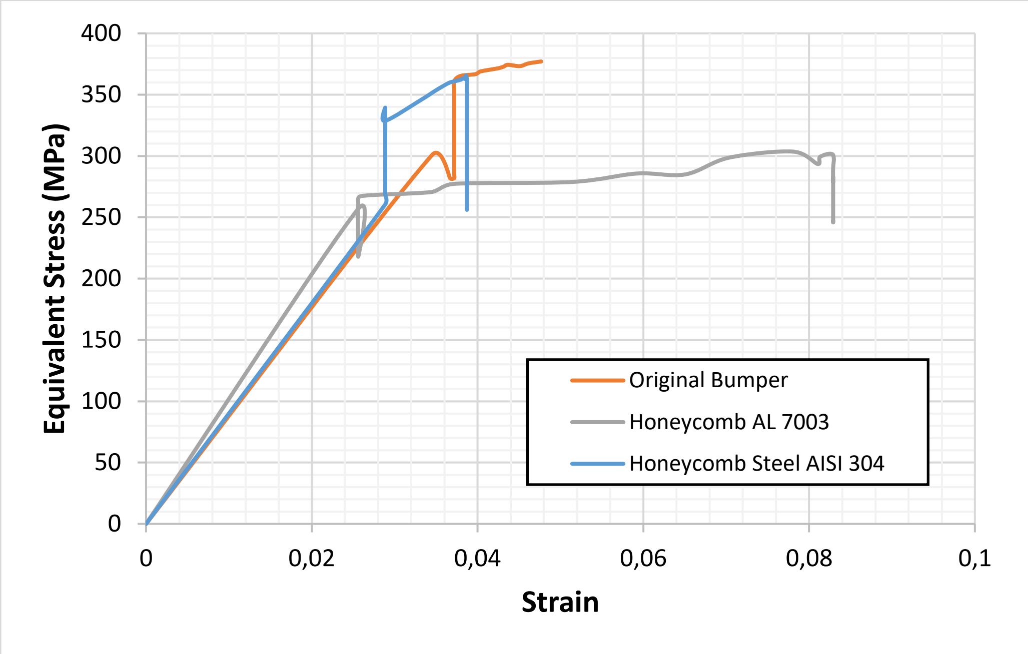

Figure 5.8: Relation Result Curve after impact for Equivalent stress and Equivalent strain.

Table 5.1: Shows The Maximum And Minimum Value Over Time For (The Total Of Deformation, Stress Of Equivalent, The Plastic Strain And Elastic Strain Equivalent).

Object Name	***Total Deformation***	***Equivalent Elastic Strain***	***Equivalent Stress***	***Equivalent Plastic Strain***
Definition				
Original Bumper				
Maximum Value Over Time				
Minimum	0. mm	0. mm/mm	0. MPa	0. mm/mm
Maximum	45.27 mm	0.0019 mm/mm	377.07 MPa	0.0476 mm/mm
Honeycomb Steel AISI 304 Bumper				
Maximum Value Over Time				
Minimum	0. mm	0. mm/mm	0. MPa	0. mm/mm
Maximum	22.36 mm	0.00135 mm/mm	256.07 MPa	0.0387 mm/mm
Honeycomb AL 7003 Bumper				
Maximum Value Over Time				
Minimum	0. mm	0. mm/mm	0. MPa	0. mm/mm
Maximum	35.69 mm	0.0036 mm/mm	247.45 MPa	0.0828 mm/mm

5.1.2 Natural Frequency Studies

Frequency studies are conducted to compute resonant frequencies and the corresponding mode shapes. When a body is subjected to a vibrating environment, frequency studies can prevent failure related to resonance-induced excessive stresses. When a body is disturbed from its resting state, it tends to vibrate at natural or resonant frequencies. The fundamental frequency refers to the lowest natural frequency. The body takes a certain shape for each natural frequency; this is called the mode shape. The three-mode shape for the design of each bumper is shown in figure (4-11), (4-12) and (4-13) at the lowest natural frequency for the original bumper, honeycomb (Steel AISI 304) bumper, and honeycomb (AL7003) bumper the value is (232.11 Hz, 247.02 Hz and 252.29 Hz, respectively). Also, the figures illustrate the effect of natural frequencies on bumper design, and how this effect appears in the form of total deformation.

5.2 EXPERIMENTAL DISCUSSION

Using a brand new 2019 KIA Optima as an example, Figure (4-14) displays the force-deformation curve obtained under quasi-static conditions. As the impact bar smashed the bumper, it eventually gave way, and the bumper was destroyed. During the compression phase of the curve, the plastic energy absorber is crushed at the first symptoms of deformation (39.139 mm). The force-deformation curve of the plastic energy absorber steepened as it was distorted. After the force peaked at around 8000 N, the impact bar fractured under the compression strain and the force slowly declined.

5.3 CONCLUSION

In this research, three bumper cases were tested in full-size crashes and high-speed velocity impacts. The crashworthiness of the three FE models was studied using nonlinear finite element explicit dynamics. Numerical results confirmed the bionic bumper models significantly improved crashworthiness.

The following are the key conclusions drawn from this work:

a. When compared to the original bumper, the enhanced bionic bumper has a 15.2 % increase in internal absorber energy. Additionally, plastic energy is high at approximately 18%.
b. The honeycomb bumper (Steel AISI 304) beam is more resistant to deformation than apparent throughout the impact period, with total deformation reduced by approximately 47.18 % when compared to the original bumper.
c. The honeycomb bumper (AL 7003) beam is more resistant to deformation than apparent throughout the impact period, with total deformation reduced by approximately 11.58% when compared to the original bumper.
d. The change of equivalent elastic and plastic stain demonstrates the stress concentration and plastic deformation caused by the rigid wall.

e. The percentage of reduction in equivalent plastic strain for the honeycomb bumper (Steel AISI 304) compared with the original bumper is about 19%.

f. This research established that the natural frequencies from the numerical results are relatively close to each other for most of the modes, that increasing the cross-section area of the honeycomb raised the natural frequency by making the model stiffer, and that increasing the natural frequency was also achieved by using curves instead of sharp corners.

g. The Honeycomb AL 7003 give redaction in wight compared to models in which Steel AISI 304 was used, where the percentage of reduction ranged from 49 %.

h. The experiment test was illustrating the original bumper crash behaver at static load impact Therefore, in order to take an overview of the deformation that occurs in the bumper of a car when hitting a rigid wall.

5.4 RECOMMENDATIONS FOR FUTURE WORK

The following suggestions are recommended for future work:

a. Add materials to the hollow aluminum bumper and fill it with (Foam) or (FGF) in order to increase the absorption because one of the most important objectives of the BUMPER is to increase the absorption and reduce the transmission of the collision to the rest of the car parts in addition to maintaining its weight

b. Made a prototype for the Original Bumper to optimize the bumper with different material.

c. Relying on more than one bionic design simulation, in which patterns similar to animals or plants are used, and a comparison is made between them.

d. Using composite materials and fiberglass instead of the base metals used in the automobile industry.

e. Simulate the collision of the two cases, high velocity and low velocity, and compare them.

f. Carrying out a crash test is experimental in a university if it is available.

REFERENCES

[1] F. Rosenthal, R. L. Bert, G. J. O'Hara, E. W. Clements, and R. A. Skep, "The Mechanics of Automobile Collisions," NAVAL RESEARCH LAB WASHINGTON DC, 1972.

[2] A. Ghadianlou and A. Farhaninejad, "Crashworthiness evaluation of vehicle side door beam by material investigation and geometry modification in side impacts," in *International ASET INC.*, 2012, no. 38.

[3] T. Xu, N. Liu, Z. Yu, T. Xu, and M. Zou, "Crashworthiness Design for Bionic Bumper Structures Inspired by Cattail and Bamboo," *Appl Bionics Biomech*, vol. 2017, 2017, doi: 10.1155/2017/5894938.

[4] *Mechanobiology Handbook, Second Edition*. 2018. doi: 10.1201/9780429444982.

[5] H. Zarei, M. Kröger, and H. Albertsen, "An experimental and numerical crashworthiness investigation of thermoplastic composite crash boxes," *Compos Struct*, vol. 85, no. 3, 2008, doi: 10.1016/j.compstruct.2007.10.028.

[6] C. Y. Wang, W. W. Wang, W. Z. Zhao, Y. Wang, and G. Zhou, "Structure design and multi-objective optimization of a novel NPR bumper system," *Compos B Eng*, vol. 153, 2018, doi: 10.1016/j.compositesb.2018.07.024.

[7] J. J. Blum *et al.*, "Vehicle related factors that influence injury outcome in head-on collisions," in *Annals of Advances in Automotive Medicine - 52nd Annual Scientific Conference*, 2008, vol. 52.

[8] "The Physics of a Car Collision." https://www.thoughtco.com/what-is-the-physics-of-a-car-collision-2698920 (accessed Sep. 09, 2022).

[9] S. ÖZEL, S. KARAGÖZ, and H. BEYTÜT, "CRASHWORTHINESS INVESTIGATION OF VEHICLE FRONT BUMPER BEAM WITH DIFFERENT CROSS-SECTIONS UNDER AXIAL DYNAMIC LOAD," *European Journal of Technic*, 2020, doi: 10.36222/ejt.625873.

[10] "Wholesale Kia OEM Parts | Kia Parts Store." https://www.kia.parts/ (accessed Jun. 09, 2022).

[11] F. Mo, S. Zhao, C. Yu, Z. Xiao, and S. Duan, “Design of a Conceptual Bumper Energy Absorber Coupling Pedestrian Safety and Low-Speed Impact Requirements,” *Appl Bionics Biomech*, vol. 2018, 2018, doi: 10.1155/2018/9293454.

[12] “2019 Kia Optima Specifications.” https://www.kiamedia.com/us/en/models/optima/2019/specifications (accessed May 28, 2022).

[13] “A Complete List of Car Body Parts [Names & Functions] PDF.” https://www.theengineerspost.com/parts-of-car-body/ (accessed Sep. 14, 2022).

[14] A. Nowak and W. Rokicki, “Bionic forms in search of structural models in architecture,” in *MATEC Web of Conferences*, 2018, vol. 174. doi: 10.1051/matecconf/201817403020.

[15] N. K. Katiyar, G. Goel, S. Hawi, and S. Goel, “Nature-inspired materials: Emerging trends and prospects,” *NPG Asia Materials*, vol. 13, no. 1. 2021. doi: 10.1038/s41427-021-00322-y.

[16] “CENIT CAD Tools Enable AM-Based Bionic Aircraft Design - Digital Engineering 24/7.” https://www.digitalengineering247.com/article/cenit-cad-tools-enable-am-based-bionic-aircraft-design (accessed Sep. 14, 2022).

[17] “2019 Kia Optima Specifications.” https://www.kiamedia.com/us/en/models/optima/2019/specifications (accessed Jun. 09, 2022).

[18] D. T. Detwiler and R. A. Miller, “Development of a sport utility front bumper system for pedestrian safety and 5 mph impact performance,” SAE Technical Paper, 2001.

[19] R. Tanov, M. Brueggert, and S. Yang, “Finite element modeling and crash analysis of a school bus,” in *SAE Technical Papers*, 2003. doi: 10.4271/2003-01-3425.

[20] J. W. Lee, K. H. Yoon, Y. S. Kang, and G. J. Park, “Vehicle hood and bumper structure design to mitigate casualties of pedestrian accidents,” *ESV -Paper no. 05-0105*, no. February, 2005.

[21] R. Hosseinzadeh, M. M. Shokrieh, and L. B. Lessard, “Parametric study of automotive composite bumper beams subjected to low-velocity impacts,” *Compos Struct*, vol. 68, no. 4, 2005, doi: 10.1016/j.compstruct.2004.04.008.

[22] S. Kokkula, O. S. Hopperstad, O. G. Lademo, T. Berstad, and M. Langseth, “Offset impact behaviour of bumper beam-longitudinal systems: Numerical simulations,” *International Journal of Crashworthiness*, vol. 11, no. 4, 2006, doi: 10.1533/ijcr.2005.0106.

[23] H. R. Zarei and M. Kröger, “Bending behavior of empty and foam-filled beams: Structural optimization,” *Int J Impact Eng*, vol. 35, no. 6, 2008, doi: 10.1016/j.ijimpeng.2007.05.003.

[24] M. K. Shin, S. I. Yi, O. T. Kwon, and G. J. Park, “Structural optimization of the automobile frontal structure for pedestrian protection and the low-speed impact test,” *Proceedings of the Institution of Mechanical Engineers, Part D: Journal of Automobile Engineering*, vol. 222, no. 12, 2008, doi: 10.1243/09544070JAUTO788.

[25] M. M. Davoodi, S. M. Sapuan, and R. Yunus, “Conceptual design of a polymer composite automotive bumper energy absorber,” *Mater Des*, vol. 29, no. 7, 2008, doi: 10.1016/j.matdes.2007.07.011.

[26] J. Marzbanrad, M. Alijanpour, and M. S. Kiasat, “Design and analysis of an automotive bumper beam in low-speed frontal crashes,” *Thin-Walled Structures*, vol. 47, no. 8–9, 2009, doi: 10.1016/j.tws.2009.02.007.

[27] Z. Zhang, S. Liu, and Z. Tang, “Design optimization of cross-sectional configuration of rib-reinforced thin-walled beam,” *Thin-Walled Structures*, vol. 47, no. 8–9, 2009, doi: 10.1016/j.tws.2009.02.009.

[28] T. van Langenhove, L. Farkas, C. Canadas, S. Donders, J. Tielens, and D. Schildermans, “Optimization study of a parametric (CAD) vehicle bumper subsystem under multiple load cases using LMS Virtual. Lab”.

[29] D. K. Park, C. D. Jang, S. B. Lee, S. J. Heo, H. J. Yim, and M. S. Kim, “Optimizing the shape of a bumper beam section considering pedestrian protection,” *International Journal of Automotive Technology*, vol. 11, no. 4, 2010, doi: 10.1007/s12239-010-0060-y.

[30] W. R. Scott, C. Bain, S. J. Manoogian, J. M. Cormier, and J. R. Funk, “Simulation model for low-speed bumper-to-bumper crashes,” in *SAE Technical Papers*, 2010. doi: 10.4271/2010-01-0051.

[31] M. M. Davoodi, S. M. Sapuan, D. Ahmad, A. Aidy, A. Khalina, and M. Jonoobi, "Concept selection of car bumper beam with developed hybrid bio-composite material," *Mater Des*, vol. 32, no. 10, 2011, doi: 10.1016/j.matdes.2011.06.011.

[32] A. R. M. Moghaddam and M. T. Ahmadian, "Design and analysis of an automobile bumper with the capacity of energy release using GMT materials," *World Academy of Science, Engineering and Technology, International Journal of Mechanical, Aerospace, Industrial, Mechatronic and Manufacturing Engineering*, vol. 5, no. 4, 2011.

[33] R. R. Magalhaes, C. H. O. Fontes, and S. A. B. Vieira De Melo, "Stress analysis of a front bumper fascia using the boundary element method," *Eng Anal Bound Elem*, vol. 36, no. 8, 2012, doi: 10.1016/j.enganabound.2012.02.008.

[34] L. Farkas, D. Moens, S. Donders, and D. Vandepitte, "Optimisation study of a vehicle bumper subsystem with fuzzy parameters," *Mech Syst Signal Process*, vol. 32, 2012, doi: 10.1016/j.ymssp.2011.11.014.

[35] N. Tanlak, F. Ö. SÖNMEZ, and M. Şenaltun, "Shape optimization of beams under transverse crash," *no. June*, vol. 2012, 2012.

[36] E. Koricho, G. Belingardi, A. Tekalign, D. Roncato, and B. Martorana, "Crashworthiness Analysis of Composite and Thermoplastic Foam Structure for Automotive Bumper Subsystem," in *Advanced Composite Materials for Automotive Applications: Structural Integrity and Crashworthiness*, 2013. doi: 10.1002/9781118535288.ch6.

[37] N. Tanlak, F. O. Sonmez, and M. Senaltun, "Shape optimization of bumper beams under high-velocity impact loads," *Eng Struct*, vol. 95, 2015, doi: 10.1016/j.engstruct.2015.03.046.

[38] E. S. Roopesh and L. B. Rao, "Design and Analysis of an Automotive Frontal Bumper Beam for Low-Speed Crashes," *Journal of Multidisciplinary Engineering Science and Technology (JMEST)*, vol. 2, pp. 994–998, 2015.

[39] P. Sampath Rao, "DESIGN ANALYSIS OF BUMPER BEAM SUBJECTED TO OFFSET IMPACT LOADING FOR AUTOMOTIVE APPLICATIONS," *International Journal of Mechanical Engineering and Technology*, vol. 6, no. 5, 2015.

[40] Z. Xiao, J. Fang, G. Sun, and Q. Li, “Crashworthiness design for functionally graded foam-filled bumper beam,” *Advances in Engineering Software*, vol. 85, 2015, doi: 10.1016/j.advengsoft.2015.03.005.

[41] P. R. Reddy and T. Harish, “Design and crash analysis of passenger car frontal bumper beam using Hypermesh and Radioss,” *International Journal of Emerging Research in Management & Technology*, vol. 2, 2015.

[42] M. v Dange, R. B. Buktar, and N. R. Raykar, “Design and Analysis of an Automotive Front Bumper Beam for Low-Speed Impact,” *IOSR Journal of Mechanical and Civil Engineering Ver*, vol. 12, no. 2, 2015.

[43] Z. Li, Q. Yu, X. Zhao, M. Yu, P. Shi, and C. Yan, “Crashworthiness and lightweight optimization to applied multiple materials and foam-filled front end structure of auto-body,” *Advances in Mechanical Engineering*, vol. 9, no. 8, 2017, doi: 10.1177/1687814017702806.

[44] C. R. Sonawane and A. L. Shelar, “Strength Enhancement of Car Front Bumper for Slow Speed Impact by FEA Method as per IIHS Regulation,” *Journal of The Institution of Engineers (India): Series C*, vol. 99, no. 5, 2018, doi: 10.1007/s40032-017-0365-y.

[45] J. Fu, Q. Liu, K. Liufu, Y. Deng, J. Fang, and Q. Li, “Design of bionic-bamboo thin-walled structures for energy absorption,” *Thin-Walled Structures*, vol. 135, 2019, doi: 10.1016/j.tws.2018.10.003.

[46] M. P. Wagh and O. A. More, “Vibration and Impact Analysis of Optimized Automotive Front Bumper,” *International Journal of Engineering Research & Technology (IJERT)*, vol. 9, pp. 1370–1379, 2020.

[47] W. Johnson, “The Elements of Crashworthiness: Scope and Actuality,” *Proceedings of the Institution of Mechanical Engineers, Part D: Journal of Automobile Engineering*, vol. 204, no. 4, 1990, doi: 10.1177/095440709020400406.

[48] W. Johnson, S. R. Reid, and T. Y. Reddy, “The compression of crossed layers of thin tubes,” *Int J Mech Sci*, vol. 19, no. 7, 1977, doi: 10.1016/0020-7403(77)90042-X.

[49] W. Johnson and S. R. Reid, “METALLIC ENERGY DISSIPATING SYSTEMS.,” *Appl Mech Rev*, vol. 31, no. 3, 1978.

[50] W. Johnson, “STRUCTURAL DAMAGE IN AIRSHIP AND ROLLING STOCK COLLISIONS.,” 1983.

[51] W. Johnson and A. C. Walton, “An experimental investigation of the energy dissipation of a number of car bumpers under quasi-static lateral loads,” *Int J Impact Eng*, vol. 1, no. 3, 1983, doi: 10.1016/0734-743X(83)90024-6.

[52] L. Zhang, *Engineering Plasticity And Impact Dynamics, Proceedings Of The Intl Symp On Plasticity And Impact (Ispi 2001)*. World Scientific, 2001.

[53] T. Yu and L. Zhang, *Plastic bending: theory and applications*, vol. 2. World Scientific, 1996.

[54] A. S. Khan and S. Huang, *Continuum theory of plasticity*. John Wiley & Sons, 1995.

[55] A. Partovi and S. S. Shamili, “Analysis of autofrettaged high pressure components.” 2012.

[56] N.-H. Kim, *Introduction to nonlinear finite element analysis*. Springer Science & Business Media, 2014.

[57] R. Sunder, S. A. Seetharam, and T. A. Bhaskaran, “Cycle counting for fatigue crack growth analysis,” *Int J Fatigue*, vol. 6, no. 3, pp. 147–156, 1984.

[58] D. L. Logan, *A first course in the finite element method*. Cengage Learning, 2016.

[59] M. M. Gauthier, *Engineered materials handbook*, vol. 1. ASM International, 1995.

[60] H. Sutherland and J. Mandell, “Optimized Goodman Diagram for the Analysis of Fiberglass Composites Used in Wind Turbine Blades,” in *43rd AIAA Aerospace Sciences Meeting and Exhibit*, 2005, p. 196.

[61] A. E. Masich, “Rodman’s Big Gun,” *Western Pennsylvania History: 1918-2018*, pp. 20–31, 2015.

[62] “What is kinetic energy? (article) | Khan Academy.” https://www.khanacademy.org/science/physics/work-and-energy/work-and-energy-tutorial/a/what-is-kinetic-energy (accessed Sep. 27, 2022).

[63] "Internal Energy: Definition, Formula & Change | StudySmarter." https://www.studysmarter.co.uk/explanations/physics/particle-model-of-matter/internal-energy/ (accessed Sep. 27, 2022).

[64] M. T. Islam and E. A. Singh, "Study of behavior of RCC beam under impact loading and effect of hourglass energy by finite element analysis using ANSYS," *IJERT*, vol. 8, no. 07, pp. 2181–2278, 2019.

[65] H. A. Radi and J. O. Rasmussen, *Principle of Physics for Scientists and Engineers*. 2013.

[66] D. Tongqiang, "Research on the theory model and method of accident reconstruction," *Changchun: Jilin University*, 2005.

[67] C. Ge, P. Yulong, and Z. Zhongyi, "Reconstruction analysis model for automobile-motorcycle collision accidents," *China Safety Science Journal*, vol. 24, no. 9, pp. 46–52, 2014.

[68] H. Chi and B. Gong, "Analysis of energy conversion law in vehicle collision accident," in *Journal of Physics: Conference Series*, 2020, vol. 1486, no. 7, p. 072014.

[69] E. R. Teoh and A. K. Lund, "IIHS side crash test ratings and occupant death risk in real-world crashes," *Traffic Inj Prev*, vol. 12, no. 5, pp. 500–507, 2011.

[70] D. Vangi, "Energy loss in vehicle to vehicle oblique impact," *Int J Impact Eng*, vol. 36, no. 3, pp. 512–521, 2009.

[71] F. Rosenthal, R. L. Bert, G. J. O'Hara, E. W. Clements, and R. A. Skep, "The Mechanics of Automobile Collisions," NAVAL RESEARCH LAB WASHINGTON DC, 1972.

[72] L. Wahl, S. Maas, D. Waldmann, A. Zürbes, and P. Frères, "Shear stresses in honeycomb sandwich plates: Analytical solution, finite element method and experimental verification," *Journal of Sandwich Structures and Materials*, vol. 14, no. 4, 2012, doi: 10.1177/1099636212444655.

[73] L. Hu, F. You, and T. Yu, "Effect of cell-wall angle on the in-plane crushing behaviour of hexagonal honeycombs," *Mater Des*, vol. 46, pp. 511–523, 2013.

[74] "AISI 304 (1.4301) Stainless Steel - Matmatch." https://matmatch.com/learn/material/aisi-304-stainless-steel (accessed Sep. 30, 2022).

[75] "EN 573-3 Grade AW-7003 T6 - 7000 Series - Matmatch." https://matmatch.com/materials/alky2049-en-573-3-grade-aw-7003-t6 (accessed Sep. 30, 2022).

[76] J. N. Reddy, *Introduction to the finite element method*. McGraw-Hill Education, 2019.

[77] S. R. Wu and J. Cheng, "Advanced development of explicit FEA in automotive applications," *Comput Methods Appl Mech Eng*, vol. 149, no. 1–4, pp. 189–199, 1997.

[78] "Why do FEA engineers use 1D, 2D, 3D elements ? - FEA for All." https://feaforall.com/why-do-fea-engineers-use-1d-2d-3d-elements/ (accessed Oct. 24, 2022).

[79] P. Rugarli, *Structural analysis with finite elements*. 2010.

[80] "Implicit vs Explicit Numerical Methods | CFD-101 by Dr. CW. Tony Hirt." https://www.flow3d.com/resources/cfd-101/numerical-issues/implicit-versus-explicit-numerical-methods/ (accessed Oct. 24, 2022).

[81] X. Chen and Y. Liu, *Finite element modeling and simulation with ANSYS Workbench*. CRC press, 2018.